

# UNVEILING THE BASIN-LIKE LOSS LANDSCAPE IN LARGE LANGUAGE MODELS

Huanran Chen<sup>1</sup>, Yinpeng Dong<sup>1</sup>, Zeming Wei<sup>2</sup>, Yao Huang<sup>1</sup>, Yichi Zhang<sup>1</sup>,  
Hang Su<sup>1</sup>, Jun Zhu<sup>1</sup>

<sup>1</sup>Tsinghua University, <sup>2</sup>Peking University  
huanran.chen@outlook.com

## ABSTRACT

We discover the emergence of *basins* in the loss landscape of large language models. As model scale increases, LLMs become progressively more resilient to random perturbations in the parameter space, giving rise to expansive stability regions where models exhibit nearly identical performance, but outside of which their capabilities collapse. We observe that pre-training creates a *basic capability* basin, and subsequent alignment fine-tuning forms *specific capability* basins (e.g., safety, math, coding). Thus, we argue that benign fine-tuning confined to the basin should preserve prior capabilities. Besides, we also analyze the loss landscape for worst-case directions, which is consistently sharp and detrimental. We find that adversarial fine-tuning moves along the nearly worst-case directions, thus rapidly degrading model capabilities. Finally, we provide a theoretical analysis demonstrating that the basin size bounds the performance degradation of any fine-tuning, including the adversarial ones, while also guaranteeing the model robustness w.r.t. input perturbations, suggesting the benefit of enlarging basins.

## 1 INTRODUCTION

Large Language Models (LLMs) have garnered significant attention in recent years for their remarkable performance across numerous applications (OpenAI, 2023; Anthropic, 2024; Dubey et al., 2024; Liu et al., 2024a). LLMs typically undergo a pre-training phase with extensive datasets to acquire foundational knowledge, followed by multiple alignment stages using high-quality, domain-specific data to activate specialized capabilities (Brown et al., 2020; OpenAI, 2023; Ouyang et al., 2022). In this work, we investigate the intriguing *alignment brittleness* phenomenon. In particular:

- Why does fine-tuning with benign data sometimes compromise capabilities acquired during prior alignment (Qi et al., 2023; Du et al., 2024; Mukhoti et al., 2023; Bianchi et al., 2023; Lyu et al., 2024; Hsu et al., 2024; Li et al., 2025; Liu et al., 2024b)?
- Why does fine-tuning with adversarial data, even for just a few steps, destroy all capabilities of LLMs (Qi et al., 2023; Rosati et al., 2024; Wang et al., 2024a; Huang et al., 2024b; Leong et al., 2024; Huang et al., 2024a;c; Wu et al., 2025)?
- Why are LLMs easily jailbroken in white-box settings, and how does this relate to the above issues (Zou et al., 2023; Qi et al., 2024; Chen et al., 2025a; Andriushchenko et al., 2024)?

We posit that these issues can be partially explained by the loss landscape of LLMs (Li et al., 2018). To investigate this, we analyze two complementary perspectives: the **most-case landscape**, capturing capacity degradation when parameters move along most directions, and the **worst-case landscape**, reflecting degradation along the worst direction. Our main findings are summarized below.

As shown in Fig. 1, the **most-case landscape** exhibits a basin-like structure: models perform nearly identically within the basin, but rapidly lose capabilities once outside (Peng et al., 2024). This basin gradually emerges and expands as model size increases (see Fig. 7), consistent with recent evidence that LLMs are robust to common parameter perturbations (Men et al., 2024; Gromov et al., 2024; Sun et al., 2023). In particular, pre-training forms a broad “basic capability basin” that confers fundamental language and conversational skills, while subsequent alignment stages carve out narrower

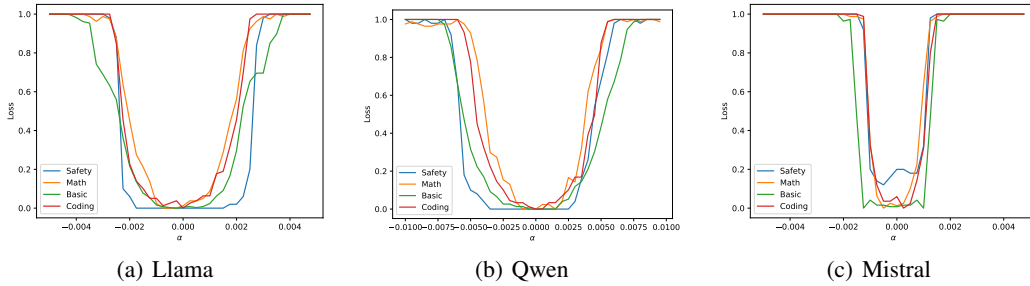


Figure 1: The most-case loss landscape of different models. Specific benchmarks and visualization details are provided in Sec. 3.2. As shown, the loss landscape of LLMs resembles a basin, within which models perform nearly identically and outside of which they lose all capabilities.

“specific capability basins” (e.g., safety, math, coding) in proximity to it. These observations suggest that *benign fine-tuning constrained within the basin preserves prior capabilities*.

As illustrated in Fig. 2, the **worst-case landscape** is consistently sharp, such that even a small fine-tuning step can move parameters outside the basin, leading to the loss of all capabilities. This resembles prior explanations for adversarial examples: in high-dimensional spaces, with high probability there exists a direction that causes rapid degradation, despite most directions being safe (Daniely & Shacham, 2020; Bubeck et al., 2021). The parameter dimensions of LLMs are significantly larger than those of earlier smaller models, making the worst-case direction potentially more detrimental. Furthermore, we argue that a lack of robustness to worst-case parameter perturbations implies vulnerability to input perturbations, such as jailbreaking. Let  $\mathbf{W}$  denote the embedding layers. Given that the embedding layers of current LLMs are onto transformations (i.e.,  $\mathbf{W}$  is column full-rank) (Carlini et al., 2024), if there exists a perturbation  $\delta_{\mathbf{W}}$  such that the model with weights  $\mathbf{W} + \delta_{\mathbf{W}}$  is not robust, there always exists an input perturbation  $\delta_{\mathbf{x}}$  such that the model at input  $\mathbf{x} + \delta_{\mathbf{x}}$  is not robust, as  $\mathbf{W}\mathbf{x} + \delta_{\mathbf{W}}\mathbf{x}$  and  $\mathbf{W}\mathbf{x} + \mathbf{W}\delta_{\mathbf{x}}$  can yield the same output (Zhang et al., 2024a). This explains LLM vulnerabilities to both jailbreaking (Zou et al., 2023) and fine-tuning attacks (Qi et al., 2023).

Through above exploratory studies, we construct a smooth model such that *the performance degradation along the worst-case direction is theoretically bounded by the size of the most-case basin*. This implies that we can derive a theoretical bound on performance degradation for *any fine-tuning* and input jailbreaking. Together with our conjecture that benign fine-tuning preserves capabilities within the most-case basin, we conclude that enlarging the most-case basin ❶ enhances benign fine-tuning, ❷ mitigates adversarial fine-tuning, and ❸ improves robustness against input jailbreaking. Additionally, we demonstrate that *the basins can be readily enlarged* during pre-training, likely due to the over-parameterization property of neural networks (Belkin et al., 2019; Allen-Zhu et al., 2019). We hope that our work sheds light on the relationships between loss landscapes, robustness to benign and harmful fine-tuning, jailbreaking, and our proposed theoretical lower bounds and optimization strategies inspire future large-scale studies on pre-training and fine-tuning.

## 2 BACKGROUND: ALIGNMENT BRITTLINESS OF LLMs

The alignment of LLMs plays a crucial role in ensuring adherence to safety and ethical standards in their applications (Anwar et al., 2024; Wang et al., 2024b; Ji et al., 2023). During the early stages of LLM advancement, researchers developed various paradigms, like reinforcement learning (Dai et al., 2024; Bai et al., 2022) or red-teaming (Perez et al., 2022; Mehrabi et al., 2023), to build their alignment, which was initially believed to be sufficient to solve the alignment problems. However, a series of recent discoveries revealed that the current alignment of LLMs is shallow and superficial (Wei et al., 2023a; Qi et al., 2023; Yang et al., 2023; Zou et al., 2023; Qi et al., 2024; Zhang et al., 2024b). Although models exhibit aligned behavior in regular settings, their alignment can be easily compromised during fine-tuning or inference, particularly in the following three aspects.

**Normal fine-tuning**<sup>1</sup>. Supervised Fine-Tuning (SFT) on task-specific datasets has become a common paradigm for adapting pre-trained LLMs to various downstream applications. However, when

<sup>1</sup>This is what previous work called “benign fine-tuning”. In this paper, benign fine-tuning refers to another type of fine-tuning defined in Sec. 3.4

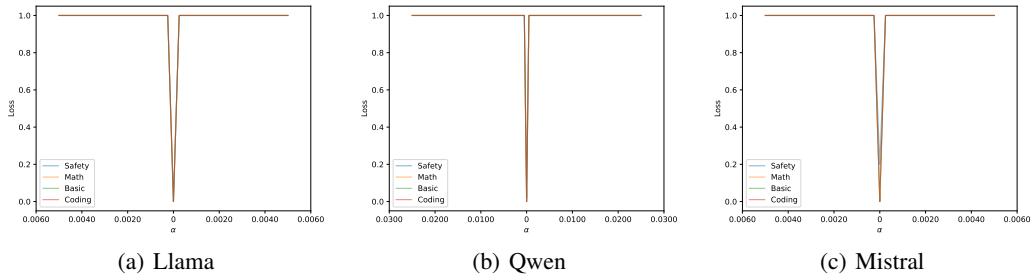


Figure 2: The worst-case loss landscape of different models. Specific benchmarks and visualization details are provided in Sec. 3.3. As shown, moving even a small distance along the worst-case direction rapidly degrades all capabilities of LLMs. Due to all curves reaching the maximum loss at the smallest scale, they completely overlap.

applied to models that have undergone alignment procedures (such as RLHF or constitutional AI), such fine-tuning may cause significant alignment degradation. For example, the Llama2-7B model raises their harmfulness response rate from 5.5% to 31.8% after fine-tuning on the Alpaca dataset with only one epoch (Qi et al., 2023).

**Adversarial fine-tuning.** Furthermore, this superficial alignment can be easily subverted with only a small amount of adversarial data. Exploiting inherent vulnerabilities in LLM alignment, malicious actors can fine-tune models on harmful examples, such as instructions promoting unsafe behavior or identity manipulation, to break safety guarantees. For instance, fine-tuning GPT-3.5 on a maliciously crafted dataset of just 10 harmful examples for 5 epochs can raise the harmfulness rate from 1.8% to 88.8% (Qi et al., 2023), effectively breaking the safety mechanisms of aligned LLMs.

**Input jailbreaking.** LLMs also suffer from input-space attacks, which are known as jailbreaking attacks. For example, adversaries can utilize optimization-based methods (Zou et al., 2023) to induce the model to answer harmful outputs, even in black-box settings (Wei et al., 2023b; Chao et al., 2023; Chen et al., 2025c; Huang et al., 2025).

Overall, these threads of discoveries suggest that the current alignment of LLMs is still overly brittle, posing significant concerns regarding their trustworthiness in real-world applications.

### 3 A CLOSER LOOK AT THE LOSS LANDSCAPE OF LLMs

In this work, we explore the above problems from the loss landscape perspective, which has verified its effectiveness in understanding the dynamics of deep networks (Li et al., 2018; Peng et al., 2024).

#### 3.1 VISUALIZATION OF THE LOSS LANDSCAPE

The loss landscape visualizes the performance change of a neural network w.r.t. parameter perturbations. Formally, let  $f_{\theta}$  denote a language model with parameters  $\theta \in \mathbb{R}^d$ , and let  $J_{f, \mathcal{D}}$  represent the benchmark functional on a dataset  $\mathcal{D}$ , defined as  $J_{f, \mathcal{D}}(\theta) := \mathbb{E}_{\mathbf{x} \in \mathcal{D}}[\mathcal{O}(f_{\theta}(\mathbf{x}))]$ , which takes  $f_{\theta}$  as input and returns a benchmark value on  $\mathcal{D}$ , characterizing its specific capability.  $\mathcal{O}$  is the judgment oracle that takes the output of  $f_{\theta}$  and returns 0 or 1 based on its correctness/safety. The higher the benchmark value  $J_{f, \mathcal{D}}(\theta)$ , the better the performance of the evaluated model  $f_{\theta}$ .

**Benchmarks.** To assess the diverse capabilities of a given model, we adopt the following benchmarks: MMLU (Hendrycks et al., 2021) for basic language proficiency, GSM8K (Cobbe et al., 2021) for mathematical reasoning, HumanEval (Mark Chen, 2021) for coding ability, and AdvBench (Zou et al., 2023) for safety performance.

**Models.** We visualize the loss landscape of three typical LLMs, including Llama-3.1-8B (Dubey et al., 2024), Qwen-2.5-7B (Yang et al., 2024) and Mistral-8B-2410 (Jiang et al., 2023). We also study the loss landscape of other models in Sec. D.

However, there are still several issues with visualizing the loss landscape. First, while lower values of loss indicate better performance, higher values of the benchmark  $J_{f, \mathcal{D}}(\theta)$  are preferable. Moreover, benchmark scores are not directly comparable across tasks (e.g., MMLU scores range from at least 0.25 and rarely exceed 0.8), which can lead to misleading interpretations. To address this, we apply

a transformation that flips the benchmark values by subtracting them from one and then normalizes them via min-max normalization. We denote this operation by  $\mathcal{T}$ , i.e., the visualized value is  $\mathcal{T} \circ J_{f,\mathcal{D}}(\theta)$ . The raw benchmark results are reported in Sec. D.2.

Besides, directly visualizing a  $d$ -dimensional landscape is computationally expensive and unintuitive (Li et al., 2018). We follow the common practice (Goodfellow et al., 2014; Im et al., 2016; Smith & Topin, 2017; Li et al., 2018): for a 2-D landscape, we visualize the loss landscape along a specific direction  $\delta \in \mathbb{R}^d$ , reducing the problem to visualizing a single-variable function:  $L(\alpha) = \mathcal{T} \circ J_{f,\mathcal{D}}(\theta + \alpha\delta)$ . For a 3-D landscape, we visualize along two random directions  $\delta_1, \delta_2 \in \mathbb{R}^d$  using  $L(\alpha, \beta) = \mathcal{T} \circ J_{f,\mathcal{D}}(\theta + \alpha\delta_1 + \beta\delta_2)$ .

In this work, we investigate two types of loss landscapes defined by the choice of direction  $\delta$ .

### 3.2 MOST-CASE LOSS LANDSCAPE

The **most-case loss landscape** adopts a uniformly random direction  $\delta \sim \mathcal{N}(\mathbf{0}, \mathbf{I})$  and visualizes the single-variable function:

$$L(\alpha) = \mathcal{T} \circ J_{f,\mathcal{D}}(\theta + \alpha\delta), \quad \delta \sim \mathcal{N}(\mathbf{0}, \mathbf{I}). \quad (1)$$

Empirically, we observe that different directions  $\delta \sim \mathcal{N}(\mathbf{0}, \mathbf{I})$  yield nearly identical results. Since  $\mathcal{N}(\mathbf{0}, \mathbf{I})$  represents uniformly random directions, this suggests that most directions produce similar landscapes. Therefore, we designate this as the **most-case loss landscape**.

**General Geometry.** As shown in Fig. 1, the most-case loss landscape for each capability resembles a basin, within which the models perform nearly identically, and outside of which they rapidly lose all capabilities (Peng et al., 2024). In particular, the pre-training stage creates a “basic capability basin” that endows the model with fundamental language comprehension and conversational abilities. Subsequent alignment stages sequentially establish specific capability basins (e.g., safety (Zou et al., 2023), math (Cobbe et al., 2021), coding (Mark Chen, 2021)) near this basic capability basin. More interestingly, *this “basin” phenomenon emerges and becomes larger as the model size increases*. For models like the Qwen-0.5 model, the loss landscape resembles the 0-1 loss landscape for small models in Li et al. (2018), which is continuous and smooth. When the models become bigger, the basins become more significant and easier to observe. Based on this observation, we argue that *as long as subsequent benign fine-tuning remains within the basin of a specific capability, the parameters will remain within this basin and thus will not compromise those capabilities*.

**Model- and Data-Specific Geometry.** As demonstrated, some basins are sufficiently large to match the size of the basic capability basin (e.g., safety in Llama and Qwen), while others are smaller (e.g., coding in Llama and Qwen). This suggests that, in these models, coding capabilities are more likely to be forgotten than other capabilities during benign fine-tuning. The size of subsequent alignment basins is model-dependent and hyperparameter-dependent. For instance, the safety basin matches the size of the basic capability basin in Llama and Qwen, but it is significantly smaller in Mistral, indicating that Mistral may be more prone to compromising safety when fine-tuned on new datasets.

**The Loss Landscape Literally Forms Basins.** The loss landscape is not a flat quadratic function but **literally** forms basins. As shown in Table 1, within these basins, the benchmark values remain literally unchanged. This aligns with recent findings that LLMs can resist common parameter perturbations (Men et al., 2024; Gromov et al., 2024; Sun et al., 2023). Within this range, models may only alter their prediction confidence without compromising their specific capabilities.

**Hypothesis Testing.** A common concern is whether the loss landscape along several random directions can represent the geometry of a high-dimensional landscape. In fact, if a property holds across several random directions, hypothesis testing enables us to assert, with an arbitrary type-I error, the percentage of directions that satisfy this property. For example, determining the percentage of directions in a  $d$ -dimensional space that form a *literal* basin is a hypothesis testing problem aimed at obtaining a statistical lower bound for the expectation of a Bernoulli variable  $\mathbb{E}_{\delta \sim \mathcal{N}(\mathbf{0}, \mathbf{I})}[\mathbb{I}\{\mathcal{T} \circ J_{f,\mathcal{D}}(\theta + \alpha\delta) = 0\}]$ . We use the Clopper-Pearson bound here; see Sec. D.4 for detailed configurations and results.

**Disclaimer.** Note that the basin phenomenon occurs only when using generative-based benchmarks. When using likelihood-based benchmarks, the loss landscape remains smooth and continuous. See Sec. C for details. However, the loss landscape using benchmarks remains a valid loss landscape,

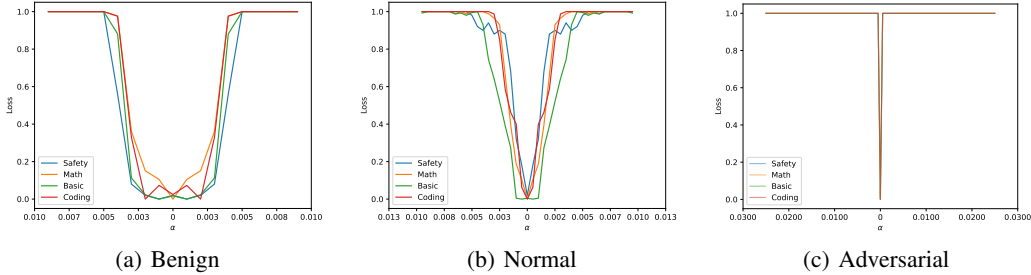


Figure 3: The SFT-case loss landscapes for three different datasets using Qwen2.5-7B.

since all benchmarks used in this paper employ a 0-1 loss on the dataset  $\mathcal{D}$ , where each sample is assigned a loss of 0/1 for a correct/incorrect response, as shown in Sec. 3.1. The landscape of 0-1 loss is widely used and studied (Keskar et al., 2017; Li et al., 2018; Garipov et al., 2018).

### 3.3 WORST-CASE LOSS LANDSCAPE

The **worst-case loss landscape** identifies the steepest direction  $\delta$  that compromises model capabilities. Formally, the worst-case direction  $\delta$  is determined by:

$$\delta = \arg \max_{\delta} L(\theta + \alpha\delta), \quad \text{s.t. } \|\delta\|_2^2 = \mathbb{E}[\|\mathcal{N}(\mathbf{0}, \mathbf{I})\|_2^2]. \quad (2)$$

The constraint  $\|\delta\|_2^2 = \mathbb{E}[\|\mathcal{N}(\mathbf{0}, \mathbf{I})\|_2^2]$  ensures that the perturbation norm matches that used in Figs. 1 and 2, enabling more direct comparison for each model. Eq. (2) is solved by optimizing  $L(\theta + b\delta)$  using SGD and projecting the norm of  $\delta$  to unity at each step (Madry et al., 2018).

**General Geometry.** As illustrated in Fig. 2, the worst-case loss landscape resembles a cliff, regardless of the model or capability evaluated. This indicates that moving a short distance along the worst-case direction rapidly degrades all model capabilities. This phenomenon aligns with prior explanations for adversarial examples: in high-dimensional spaces, with high probability there exists a worst-case direction that causes rapid degradation, despite most directions being safe (Daniely & Shacham, 2020; Bubeck et al., 2021). The parameter dimensions of large language models are significantly larger than those of earlier smaller models, making the worst-case direction potentially far more detrimental. This explains why prior adversarial fine-tuning, using only 10 samples and one epoch, can severely compromise the safety capabilities of a model (Qi et al., 2024).

### 3.4 SFT-CASE LOSS LANDSCAPE

Sec. 3.2 demonstrates that most directions do not lead to performance degradation within a certain range, whereas Sec. 3.3 shows that a worst-case direction exists that rapidly degrades all capabilities. The direction of supervised fine-tuning (SFT) naturally lies between these extremes: it may not preserve all capabilities as effectively as the most-case direction, but it does not degrade as quickly as the worst-case direction.

**Settings.** To visualize the loss landscape along the SFT direction, we select  $\delta = \frac{\theta_{sft} - \theta_0}{\|\theta_{sft} - \theta_0\|_2} \cdot \sqrt{\mathbb{E}[\|\mathcal{N}(\mathbf{0}, \mathbf{I})\|_2^2]}$ . This normalization and rescaling ensure that the perturbation norm matches those used in Secs. 3.2 and 3.3, enabling direct comparison of the loss landscapes.

**SFT Configurations.** We investigate three types of supervised fine-tuning using Qwen2.5-7B (Yang et al., 2024). *Benign fine-tuning* employs a dataset similar to the original training data. We achieve this by selecting  $\theta_0$  as Qwen2.5-7B and  $\theta_{sft}$  as its officially fine-tuned version, Qwen2.5-7B-1M (Yang et al., 2024). *Normal fine-tuning* uses a dataset with a distributional gap from the original data. We achieve this by following the setup in Section 4.4 of Qi et al. (2023), i.e., fine-tuning on the Alpaca dataset (Zheng et al., 2024) for one epoch. *Adversarial fine-tuning* utilizes the adversarial AdvBench dataset, fine-tuning for only 10 steps, following the setup in Qi et al. (2023).

**Results.** As shown in Fig. 3(a), the loss landscape along the benign fine-tuning direction resembles the most-case landscape. It preserves safety within the most-case basin and loses capability when moving outside this basin. In Fig. 3(b), when there is a distributional gap between the SFT dataset and the original dataset, the loss landscape becomes narrower and sharper, indicating that the fine-tuning direction does not align with the most-case directions. In Fig. 3(c), when fine-tuning on the

adversarial dataset, the model rapidly loses all capabilities, responding only with phrases like “Sure, here is” without providing factual answers to questions. Thus, while some SFT configurations align closely with the most-case direction (e.g., Fig. 3(a)), others deviate and degrade capabilities more rapidly (e.g., Fig. 3(b)). This variation clearly depends on the dataset and hyperparameters.

In the next section, we show that the size of the most-case basin provides a consistent bound on performance degradation, regardless of the dataset or the model’s hyperparameter sensitivity, and applies to both fine-tuning and jailbreaking attacks.

## 4 THEORETICAL BENEFITS OF BASINS

To begin, we first formally define the size of the most-case basin. We adopt a soft definition of basins, similar to the flatness definition in [Andriushchenko et al. \(2023\)](#):

**Definition 4.1** *A model  $f_{\theta}$  is said to have a  $\sigma$ -basin on benchmark  $J_{\mathcal{D}}$ , if its noised version  $f_{\theta+\epsilon}$ , where  $\epsilon \sim \mathcal{N}(\mathbf{0}, \sigma^2 \mathbf{I})$ , performs nearly the same as the original version  $f_{\theta}$ , i.e.,*

$$J_{f, \mathcal{D}}(\theta) - \mathbb{E}_{\epsilon \sim \mathcal{N}(\mathbf{0}, \sigma^2 \mathbf{I})}[J_{f, \mathcal{D}}(\theta + \epsilon)] \leq \epsilon. \quad (3)$$

Definition 4.1 is a necessary condition for a model to have a most-case landscape resembling that in Fig. 1: when  $\epsilon \rightarrow 0$ , it becomes the strict definition of basins, as defined by  $\mathbb{E}_{\delta \sim \mathcal{N}(\mathbf{0}, \mathbf{I})}[\mathbb{I}\{\mathcal{T} \circ J_{f, \mathcal{D}}(\theta + \alpha \delta) = 0\}]$  in Sec. 3.2 (assuming performance does not increase under noise perturbation). Since our theoretical analysis holds for all  $\epsilon$  rather than only  $\epsilon = 0$ , we adopt this definition in this section to provide a theoretical analysis for a more general case.

In the following section, we show that as long as a model have  $\sigma$ -basin, then we can have a (loose) guarantee the performance degradation during *any fine-tuning* and jailbreak attacks.

### 4.1 ANY ALIGNMENT CAN BE BOUNDED BY AVERAGE-CASE ALIGNMENT

This is achieved through the concept of randomized smoothing ([Cohen et al., 2019](#); [Salman et al., 2019](#); [Lee et al., 2019](#)). Since the model performs nearly identically within a  $\sigma$ -basin, for any input  $\mathbf{x}$ , instead of returning  $f_{\theta}(\mathbf{x})$ , we can sample  $\epsilon \sim \mathcal{N}(\mathbf{0}, \sigma^2 \mathbf{I})$  and return  $f_{\theta+\epsilon}(\mathbf{x})$ . Thus, the benchmark value for this model is  $J_{f, \mathcal{D}}(\theta + \epsilon)$ . The following theorem demonstrates that, for any bounded benchmark  $J_{\mathcal{D}} : \mathbb{R}^d \rightarrow [0, 1]^2$ , regardless of how sensitive  $f$  is to its parameters, the smoothed model  $\mathbb{E}_{\epsilon \sim \mathcal{N}(\mathbf{0}, \sigma^2 \mathbf{I})}[J_{f, \mathcal{D}}(\theta + \epsilon)]$  is at most  $\frac{1}{\sqrt{2\pi}\sigma}$ -Lipschitz. Consequently, when  $\theta_0$  is updated to  $\theta_{sft}$ , the benchmark value changes by at most  $\frac{1}{\sqrt{2\pi}\sigma} \|\theta_{sft} - \theta_0\|_2$ .

**Theorem 4.2** (*Weak Law of Randomized Smoothing* ([Salman et al., 2019](#))) *For any benchmark  $J_{\mathcal{D}} : \mathbb{R}^d \rightarrow [0, 1]$ , the function  $\mathbb{E}_{\epsilon \sim \mathcal{N}(\mathbf{0}, \sigma^2 \mathbf{I})}[J_{f, \mathcal{D}}(\theta + \epsilon)]$  is at most  $\frac{1}{\sqrt{2\pi}\sigma}$ -Lipschitz. Thus, we can bound the performance degradation as:*

$$\mathbb{E}_{\epsilon \sim \mathcal{N}(\mathbf{0}, \sigma^2 \mathbf{I})}[J_{f, \mathcal{D}}(\theta_{sft} + \epsilon)] \geq \mathbb{E}_{\epsilon \sim \mathcal{N}(\mathbf{0}, \sigma^2 \mathbf{I})}[J_{f, \mathcal{D}}(\theta_0 + \epsilon)] - \frac{1}{\sqrt{2\pi}\sigma} \cdot \|\theta_{sft} - \theta_0\|_2. \quad (4)$$

**Intuition.** The Lipschitz constant with respect to parameters equals the maximum gradient norm with respect to parameters. Although the gradient of a neural network cannot be bounded, the Gaussian-smoothed form transfers the gradient operator from the neural network to the probability density function of the Gaussian distribution, thereby bounding the maximum gradient norm.

[Cohen et al. \(2019\)](#); [Salman et al. \(2019\)](#) also provide a stronger version by considering the maximum Lipschitz constant at each point rather than across the entire input space, as presented in Theorem 4.3. Consequently, Theorem 4.3 consistently provides a tighter bound than Theorem 4.2.

**Theorem 4.3** (*Strong Law of Randomized Smoothing* ([Cohen et al., 2019](#); [Salman et al., 2019](#); [Lee et al., 2019](#); [Chen et al., 2025a](#))) *For any benchmark  $J_{\mathcal{D}} : \mathbb{R}^d \rightarrow [0, 1]$ , we have:*

$$\mathbb{E}_{\epsilon \sim \mathcal{N}(\mathbf{0}, \sigma^2 \mathbf{I})}[J_{f, \mathcal{D}}(\theta_{sft} + \epsilon)] \geq \Phi \left( \Phi^{-1} \left( \mathbb{E}_{\epsilon \sim \mathcal{N}(\mathbf{0}, \sigma^2 \mathbf{I})}[J_{f, \mathcal{D}}(\theta_0 + \epsilon)] \right) - \frac{\|\theta_{sft} - \theta_0\|_2}{\sigma} \right), \quad (5)$$

<sup>2</sup>Without loss of generality, any benchmark with a bounded output range can be normalized to this interval to obtain a corresponding certified bound.

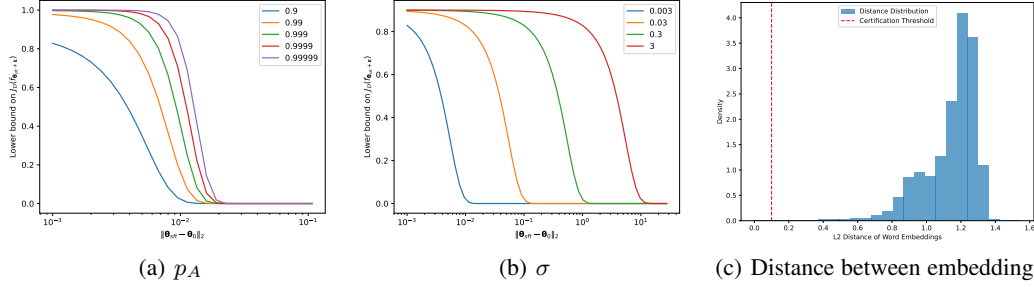


Figure 4: Lower bound guarantees. (a) The lower bound on the benchmark value of the smoothed fine-tuned model  $J_{f,\mathcal{D}}(\theta_{sft} + \epsilon)$  for varying benchmark values on the smoothed original model  $\theta_0$ , i.e.,  $p_A := \mathbb{E}_{\epsilon \sim \mathcal{N}(\mathbf{0}, \sigma^2 \mathbf{I})}[J_{f,\mathcal{D}}(\theta_0 + \epsilon)]$ , with  $\sigma = 0.003$ . (b) The lower bound on the benchmark value of the smoothed fine-tuned model  $J_{f,\mathcal{D}}(\theta_{sft} + \epsilon)$  for varying basin sizes  $\sigma$ , with  $p_A = 0.9$ . (c) Histogram of L2 distances between token embeddings.

where  $\Phi$  is the cumulative distribution function of the standard Gaussian distribution  $\mathcal{N}(0, 1)$ , i.e.,

$$\Phi(x) = \frac{1}{\sqrt{2\pi}} \int_{-\infty}^x \exp\left(-\frac{s^2}{2}\right) ds.$$

The term  $\mathbb{E}_{\epsilon}[J_{f,\mathcal{D}}(\theta + \epsilon)]$  represents the expected benchmark value when sampling  $\epsilon \sim \mathcal{N}(\mathbf{0}, \sigma^2 \mathbf{I})$  and evaluating the benchmark on  $f_{\theta+\epsilon}$ . Theorem 4.3 provides a guarantee of the expected benchmark value during fine-tuning. In practice, one typically samples a single  $\epsilon$  and evaluates  $f_{\theta+\epsilon}$ , rather than computing the expectation via extensive Monte Carlo sampling. Empirically, sampling a single instance yields results comparable to multiple samples. Theoretically, the variance introduced by sampling can be bounded using the well-known concentration phenomenon, which states that a random variable is unlikely to deviate significantly from its expectation:

**Theorem 4.4** (Concentration of Gaussian, adapted from Wainwright (2019)) *With probability at least  $1 - \delta$ , we have:*

$$J_{f,\mathcal{D}}(\theta + \epsilon) \geq \mathbb{E}_{\epsilon \sim \mathcal{N}(\mathbf{0}, \sigma^2 \mathbf{I})}[J_{f,\mathcal{D}}(\theta + \epsilon)] - L\sigma \sqrt{2 \log \frac{1}{\delta}}, \quad (6)$$

where  $L$  is the Lipschitz constant of  $J_{f,\mathcal{D}}$  with respect to  $\theta$ .

**Examples.** Through hypothesis testing in Sec. D.4, we establish that Qwen2.5-7B (Yang et al., 2024) has a  $\sigma$ -basin with  $\sigma = 0.003$  on the safety task using the AdvBench dataset, where  $\mathbb{E}_{\epsilon \sim \mathcal{N}(\mathbf{0}, \sigma^2 \mathbf{I})}[J_{f,\mathcal{D}}(\theta + \epsilon)] \geq 0.9$ . Based on this, we derive a lower bound on safety degradation as a function of  $\|\theta_{sft} - \theta_0\|_2$ . As shown in Fig. 4(a), for a  $\sigma = 0.003$  basin, a higher performance on the original parameters, i.e.,  $\mathbb{E}_{\epsilon \sim \mathcal{N}(\mathbf{0}, \sigma^2 \mathbf{I})}[J_{f,\mathcal{D}}(\theta_0 + \epsilon)]$ , yields a stronger guarantee on the fine-tuned parameters  $\theta_{sft}$ , i.e.,  $J_{f,\mathcal{D}}(\theta_{sft} + \epsilon)$ .

**Increasing the Basin Size Improves the Guarantee.** As illustrated in Fig. 4(b), enlarging the basin of a model while preserving the performance on the original model, i.e.,  $\mathbb{E}_{\epsilon \sim \mathcal{N}(\mathbf{0}, \sigma^2 \mathbf{I})}[J_{f,\mathcal{D}}(\theta + \epsilon)]$ , linearly strengthens the theoretical guarantee. In other words, increasing the basin size  $\sigma$  results in a linear improvement in the performance degradation guarantee during fine-tuning.

## 4.2 INPUT-SPACE ROBUSTNESS CAN BE BOUNDED BY MOST-CASE ALIGNMENT

In this section, we propose that the size of a basin also provides a (loose) guarantee of performance degradation against jailbreaking attacks (Zou et al., 2023; Wei et al., 2023b), by considering *only the very first layer of the model*.

**Intuition.** Let  $\mathbf{W}$  denote the embedding layers. Given that the embedding layers of current large language models are onto transformations (i.e.,  $\mathbf{W}$  is column full-rank) (Carlini et al., 2024), the activation after a weight perturbation  $\mathbf{W}\mathbf{x} + \delta_{\mathbf{W}}\mathbf{x}$ , and the activation after an input perturbation,  $\mathbf{W}\mathbf{x} + \mathbf{W}\delta_{\mathbf{x}}$ , can yield the same vector (Zhang et al., 2024a). Thus, if the model is robust to any weight perturbation  $\|\delta_{\mathbf{W}}\|_2 \leq \epsilon_{\mathbf{W}}$ , it is also robust to any input perturbation  $\delta_{\mathbf{x}}$  such that  $\mathbf{W}\delta_{\mathbf{x}} \in \{\delta_{\mathbf{W}}\mathbf{x} \mid \|\delta_{\mathbf{W}}\|_2 \leq \epsilon_{\mathbf{W}}\}$ .

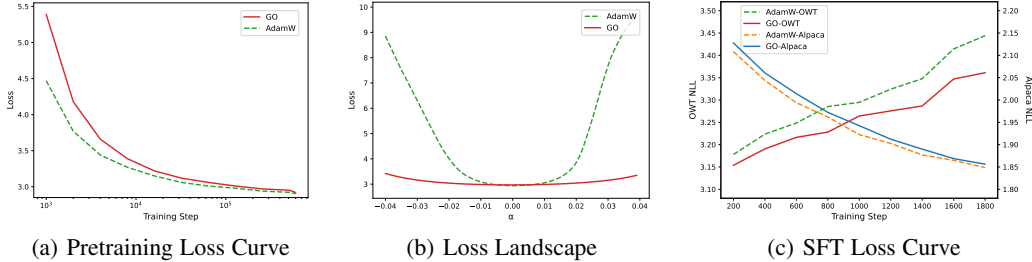


Figure 5: Pre-training and fine-tuning using GO and Adam optimizers. (a) The pre-training loss curve on OpenWebText. (b) The loss landscape on OpenWebText after pre-training. (c) Performance changes in old capability (OpenWebText) and new capability (Alpaca).

**Theorem 4.5** Let  $\mathcal{D}'$  be a modified version of  $\mathcal{D}$  where  $k$  tokens are substituted, i.e., each token  $e_i$  is replaced with  $e'_i$  in the set  $\mathcal{C} = \{(e_i, e'_i)\}_{i=1}^k$ . For any benchmark  $J_{\mathcal{D}} : \mathbb{R}^d \rightarrow [0, 1]$ , the performance degradation can be bounded by the embedding differences:

$$\mathbb{E}_{\epsilon}[J_{f, \mathcal{D}'}(\theta + \epsilon)] \geq \Phi \left( \Phi^{-1}(\mathbb{E}_{\epsilon}[J_{f, \mathcal{D}}(\theta + \epsilon)]) - \frac{\sqrt{\sum_{i=1}^k \|\mathbf{W}e_i - \mathbf{W}e'_i\|_2^2}}{\sigma} \right). \quad (7)$$

A straightforward application of this theorem involves comparing the modified and original inputs, calculating the equivalent weight differences, and applying the results from Sec. 4.1.

**Application to Certification Against Jailbreaking.** Consider  $\mathcal{D} = \{x\}$  containing a single input instance and  $J$  as a safety detector that returns values greater than 0.5 for safe outputs and less than 0.5 for harmful outputs. We can certify robustness against jailbreaking attacks by determining whether  $J_{f, \mathcal{D}'}(\theta + \epsilon)$  remains above 0.5 after modifying  $\mathcal{D} = \{x\}$  to  $\mathcal{D}' = \{x_{adv}\}$ .

We derive the following conclusions for Qwen2.5-7B (Yang et al., 2024):

**Substituting Some Tokens Preserves Performance.** Most large language models, including Qwen2.5-7B, use BPE tokenizers (Sennrich, 2015), where tokens with and without leading spaces are distinct (e.g., “hi” vs. “\_hi”). These tokens often have small  $\ell_2$  distances between each other. Special tokens, such as “<S>”, “.”, “. . .”, “ ”, and “ ”, also have small  $\ell_2$  distances. Substituting these tokens, as evaluated in Theorem 4.5, results in equivalent parameter perturbations too small to significantly alter model outputs. Thus, the model exhibits robustness to these token pairs.

**Current LLMs Are Generally Sensitive to Input Changes.** As shown in Fig. 4(c), only a small fraction of token substitutions have negligible effects on model outputs. This flexibility allows models to generate diverse responses based on input variations but also introduces robustness vulnerabilities. Minor input changes can lead to significant output variations, potentially resulting in incorrect or unsafe responses (Zou et al., 2023; Chen et al., 2025a; Andriushchenko et al., 2024).

### 4.3 BASIN MAY HAVE SUFFICIENT EXPRESSIVE POWER IN THE FUTURE

Given the theoretical guarantees of fine-tuning within a basin, one might wonder whether subsequent fine-tuning can be constrained to a theoretically guaranteed region, thereby preserving all original capabilities and achieving continual learning without forgetting (Chen et al., 2025b). A primary concern with this constraint method is whether it limits the expressive power of the hypothesis set. Specifically, if the hypothesis set is constrained to functions where  $\|\theta_{sft} - \theta_0\|_2 \leq O(\sigma)$ , can it still effectively fit the fine-tuning dataset?

We propose that *the larger the model and its basin, the greater the expressive power within the basin, enabling better acquisition of new capabilities*. As demonstrated in the following lemmas, a large model with a large basin may be even more expressive than a smaller model. Thus, in the future, one may prefer training a significantly larger model and enlarging its basin, either actively or passively (as larger models naturally form larger basins). In this case, constraining fine-tuning within the basin will provide sufficient expressive power to acquire new capabilities.

**Lemma 4.6** (Bartlett et al., 2019) *The upper and lower bounds of the VC dimension of an  $l$ -layer fully connected ReLU network are  $O(dl \log d)$  and  $\Omega(dl \log \frac{d}{l})$ , respectively.*

**Lemma 4.7** (Adapted from Neyshabur et al. (2015)) *The upper bound of the Rademacher complexity of a two-layer ReLU neural network, where each parameter has an absolute value bound of  $O(\sigma)$ , is  $O(d\sigma^2)$ .*

## 5 ENLARGING BASINS

Given that a larger basin provides stronger robustness guarantees against any fine-tuning and jail-breaking attacks, one might wonder whether the basin can be enlarged. In this section, we discover that the basin can be readily expanded, may due to the over-parameterization property of current LLMs (Liu et al., 2022; Allen-Zhu et al., 2019).

### 5.1 GAUSSIAN-AUGMENTED OPTIMIZER

As outlined in Definition 4.1, enlarging the basin size requires optimizing  $\mathbb{E}_{\epsilon \sim \mathcal{N}(\mathbf{0}, \sigma^2 \mathbf{I})} [J_{f, \mathcal{D}}(\boldsymbol{\theta} + \epsilon)]$ , ensuring that the model  $\boldsymbol{\theta}$  is robust to Gaussian perturbations. To this end, we define the loss function as the expected cross-entropy loss over perturbed parameters:

$$L_{\text{train}}(\mathbf{x}, \boldsymbol{\theta}) = -\mathbb{E}_{\epsilon \sim \mathcal{N}(\mathbf{0}, \sigma^2 \mathbf{I})} [\log p(\mathbf{x} | \boldsymbol{\theta} + \epsilon)]. \quad (8)$$

As detailed in Algorithm 1, the optimization process involves performing a forward pass with perturbed parameters  $\boldsymbol{\theta} + \epsilon$ , computing the loss, calculating the gradient via backpropagation, and using the gradient to update the parameters with a standard optimizer. We name this process GO optimizer.

### 5.2 EXPERIMENTAL RESULTS

**Settings.** To better study the effect of the GO optimizer, we applied it during pre-training. Following the NanoGPT pipeline (Karpathy, 2023), we pre-train a GPT2-127M model on OpenWebText for 600,000 steps using the same hyperparameters as in the repository. For the GO optimizer, we use identical hyperparameters, except for the additional hyperparameter  $\sigma = 0.01$ . We then fine-tune these two models on the Alpaca dataset to enhance conversational capabilities while examining performance degradation, both using the Adam optimizer.

**Pre-training Results.** As shown in Fig. 5(b), adding Gaussian noise to parameters can significantly expand the basin size. Although the GO optimizer is slower than Adam at the beginning of training, as it requires optimizing the loss across the entire neighborhood, it gradually catches up and reduces the performance gap (see Fig. 5(a)), possibly due to the over-parameterization property of current large language models. More interestingly, the GO optimizer appears to introduce some inductive bias, outperforming AdamW on some benchmarks (see Sec. D.5).

**Fine-tuning Results.** We propose that the larger the basin, the less performance degradation occurs during benign fine-tuning (since benign fine-tuning, which aims to enhance the model, should not be more harmful than Gaussian noise) and that it does not affect the acquisition of new capabilities (since larger basins imply greater expressive power within the basin). As demonstrated in Fig. 5(c), fine-tuning a model pre-trained with the Gaussian-augmented optimizer achieves significantly less performance degradation on OpenWebText while maintaining nearly the same learning speed on Alpaca, supporting this claim. See Sec. D.5 for detailed analysis of additional benchmarks.

## 6 CONCLUSION

In this work, we explore the loss landscape of large language models to elucidate the alignment brittleness phenomenon. We demonstrate that the loss landscape of large language models resembles a basin, within which models perform nearly identically and outside of which they lose all capabilities. This property enables us to derive a theoretical lower bound on performance degradation during *any fine-tuning* and jailbreaking attacks within certain norm constraints. We also show that the basin can be readily expanded due to the over-parameterization property of neural networks. Despite these contributions, our exploration remains preliminary. We hope our work sheds light on the alignment brittleness phenomenon and motivates large-scale studies that apply the GO optimizer during the pre-training phase of larger models at cutting-edge scales, verifying the practical utility of these theoretical guarantees and the relationship between basin size and performance degradation in general fine-tuning. See Sec. F for more detailed discussion.

## REFERENCES

- Samuel K Ainsworth, Jonathan Hayase, and Siddhartha Srinivasa. Git re-basin: Merging models modulo permutation symmetries. *arXiv preprint arXiv:2209.04836*, 2022.
- Zeyuan Allen-Zhu, Yuanzhi Li, and Zhao Song. A convergence theory for deep learning via over-parameterization. In *International conference on machine learning*, pp. 242–252. PMLR, 2019.
- Maksym Andriushchenko, Francesco Croce, Maximilian Müller, Matthias Hein, and Nicolas Flammarion. A modern look at the relationship between sharpness and generalization. *arXiv preprint arXiv:2302.07011*, 2023.
- Maksym Andriushchenko, Francesco Croce, and Nicolas Flammarion. Jailbreaking leading safety-aligned llms with simple adaptive attacks. *arXiv preprint arXiv:2404.02151*, 2024.
- Anthropic. The claude 3 model family: Opus, sonnet, haiku. 2024.
- Usman Anwar, Abulhair Saparov, Javier Rando, Daniel Paleka, Miles Turpin, Peter Hase, Ekdeep Singh Lubana, Erik Jenner, Stephen Casper, Oliver Sourbut, et al. Foundational challenges in assuring alignment and safety of large language models. *Transactions on Machine Learning Research*, 2024.
- Yuntao Bai et al. Constitutional ai: Harmlessness from ai feedback, 2022.
- Peter L Bartlett, Nick Harvey, Christopher Liaw, and Abbas Mehrabian. Nearly-tight vc-dimension and pseudodimension bounds for piecewise linear neural networks. *Journal of Machine Learning Research*, 20(63):1–17, 2019.
- Mikhail Belkin, Daniel Hsu, Siyuan Ma, and Soumik Mandal. Reconciling modern machine-learning practice and the classical bias–variance trade-off. *Proceedings of the National Academy of Sciences*, pp. 15849–15854, 2019.
- Federico Bianchi, Mirac Suzgun, Giuseppe Attanasio, Paul Röttger, Dan Jurafsky, Tatsunori Hashimoto, and James Zou. Safety-tuned llamas: Lessons from improving the safety of large language models that follow instructions. *arXiv preprint arXiv:2309.07875*, 2023.
- Tom Brown, Benjamin Mann, Nick Ryder, Melanie Subbiah, Jared D Kaplan, Prafulla Dhariwal, Arvind Neelakantan, Pranav Shyam, Girish Sastry, Amanda Askell, et al. Language models are few-shot learners. *Advances in neural information processing systems*, pp. 1877–1901, 2020.
- Sébastien Bubeck, Yeshwanth Cherapanamjeri, Gauthier Gidel, and Remi Tachet des Combes. A single gradient step finds adversarial examples on random two-layers neural networks. *Advances in Neural Information Processing Systems*, pp. 10081–10091, 2021.
- Nicholas Carlini, Daniel Paleka, Krishnamurthy Dj Dvijotham, Thomas Steinke, Jonathan Hayase, A Feder Cooper, Katherine Lee, Matthew Jagielski, Milad Nasr, Arthur Conmy, et al. Stealing part of a production language model. *arXiv preprint arXiv:2403.06634*, 2024.
- Patrick Chao, Alexander Robey, Edgar Dobriban, Hamed Hassani, George J Pappas, and Eric Wong. Jailbreaking black box large language models in twenty queries. In *R0-FoMo: Robustness of Few-shot and Zero-shot Learning in Large Foundation Models*, 2023.
- Huanran Chen, Yinpeng Dong, Shitong Shao, Zhongkai Hao, Xiao Yang, Hang Su, and Jun Zhu. Diffusion models are certifiably robust classifiers. In *The Thirty-eighth Annual Conference on Neural Information Processing Systems*, 2024.
- Huanran Chen, Yinpeng Dong, Zeming Wei, Hang Su, and Jun Zhu. Towards the worst-case robustness of large language models. *arXiv preprint arXiv:2501.19040*, 2025a.
- Pin-Yu Chen, Han Shen, Payel Das, and Tianyi Chen. Fundamental safety-capability trade-offs in fine-tuning large language models. *arXiv preprint arXiv:2503.20807*, 2025b.
- Taiye Chen, Zeming Wei, Ang Li, and Yisen Wang. Scalable defense against in-the-wild jailbreaking attacks with safety context retrieval. *arXiv preprint arXiv:2505.15753*, 2025c.

- Karl Cobbe, Vineet Kosaraju, Mohammad Bavarian, Mark Chen, Heewoo Jun, Lukasz Kaiser, Matthias Plappert, Jerry Tworek, Jacob Hilton, Reiichiro Nakano, Christopher Hesse, and John Schulman. Training verifiers to solve math word problems. *arXiv preprint arXiv:2110.14168*, 2021.
- Jeremy Cohen, Elan Rosenfeld, and Zico Kolter. Certified adversarial robustness via randomized smoothing. In *International Conference on Machine Learning*, pp. 1310–1320, 2019.
- Josef Dai, Xuehai Pan, Ruiyang Sun, et al. Safe rlhf: Safe reinforcement learning from human feedback. In *ICLR*, 2024.
- Amit Daniely and Hadas Shacham. Most relu networks suffer from l2 adversarial perturbations. *Advances in Neural Information Processing Systems*, pp. 6629–6636, 2020.
- Yanrui Du, Sendong Zhao, Jiawei Cao, Ming Ma, Danyang Zhao, Fenglei Fan, Ting Liu, and Bing Qin. Towards secure tuning: Mitigating security risks arising from benign instruction fine-tuning. *arXiv preprint arXiv:2410.04524*, 2024.
- Abhimanyu Dubey, Abhinav Jauhri, Abhinav Pandey, Abhishek Kadian, Ahmad Al-Dahle, Aiesha Letman, Akhil Mathur, Alan Schelten, Amy Yang, Angela Fan, et al. The llama 3 herd of models. *arXiv preprint arXiv:2407.21783*, 2024.
- Jonathan Frankle, Gintare Karolina Dziugaite, Daniel Roy, and Michael Carbin. Linear mode connectivity and the lottery ticket hypothesis. In *International Conference on Machine Learning*, pp. 3259–3269. PMLR, 2020.
- Timur Garipov, Pavel Izmailov, Dmitrii Podoprikin, Dmitry P Vetrov, and Andrew G Wilson. Loss surfaces, mode connectivity, and fast ensembling of dnns. *Advances in neural information processing systems*, 31, 2018.
- Ian J Goodfellow, Oriol Vinyals, and Andrew M Saxe. Qualitatively characterizing neural network optimization problems. *arXiv preprint arXiv:1412.6544*, 2014.
- Andrey Gromov, Kushal Tirumala, Hassan Shapourian, Paolo Glorioso, and Daniel A Roberts. The unreasonable ineffectiveness of the deeper layers. *arXiv preprint arXiv:2403.17887*, 2024.
- Dan Hendrycks, Collin Burns, Steven Basart, Andrew Critch, Jerry Li, Dawn Song, and Jacob Steinhardt. Aligning ai with shared human values. *Proceedings of the International Conference on Learning Representations (ICLR)*, 2021.
- Chia-Yi Hsu, Yu-Lin Tsai, Chih-Hsun Lin, Pin-Yu Chen, Chia-Mu Yu, and Chun-Ying Huang. Safe lora: The silver lining of reducing safety risks when finetuning large language models. *Advances in Neural Information Processing Systems*, 37:65072–65094, 2024.
- Tiansheng Huang, Sihao Hu, Fatih Ilhan, Selim Furkan Tekin, and Ling Liu. Harmful fine-tuning attacks and defenses for large language models: A survey. *arXiv preprint arXiv:2409.18169*, 2024a.
- Tiansheng Huang, Sihao Hu, Fatih Ilhan, Selim Furkan Tekin, and Ling Liu. Lazy safety alignment for large language models against harmful fine-tuning. *arXiv preprint arXiv:2405.18641*, 2024b.
- Tiansheng Huang, Sihao Hu, and Ling Liu. Vaccine: Perturbation-aware alignment for large language models against harmful fine-tuning attack. *arXiv preprint arXiv:2402.01109*, 2024c.
- Yao Huang, Yitong Sun, Shouwei Ruan, Yichi Zhang, Yinpeng Dong, and Xingxing Wei. Breaking the ceiling: Exploring the potential of jailbreak attacks through expanding strategy space. *arXiv preprint arXiv:2505.21277*, 2025.
- Daniel Jiwoong Im, Michael Tao, and Kristin Branson. An empirical analysis of deep network loss surfaces. 2016.
- Arthur Jacot, Franck Gabriel, and Clément Hongler. Neural tangent kernel: Convergence and generalization in neural networks. *Advances in Neural Information Processing Systems*, 2018.

- Jiaming Ji, Tianyi Qiu, Boyuan Chen, Borong Zhang, Hantao Lou, Kaile Wang, Yawen Duan, Zhonghao He, Jiayi Zhou, Zhaowei Zhang, et al. Ai alignment: A comprehensive survey. *arXiv preprint arXiv:2310.19852*, 2023.
- Albert Q. Jiang, Alexandre Sablayrolles, Arthur Mensch, Chris Bamford, Devendra Singh Chaplot, Diego de las Casas, Florian Bressand, Gianna Lengyel, Guillaume Lample, Lucile Saulnier, L el io Renard Lavaud, Marie-Anne Lachaux, Pierre Stock, Teven Le Scao, Thibaut Lavril, Thomas Wang, Timoth ee Lacroix, and William El Sayed. Mistral 7b. *arXiv preprint arXiv:2310.06825*, 2023.
- Andrej Karpathy, 2023. URL <https://github.com/karpathy/nanoGPT>.
- Nitish Shirish Keskar, Dheevatsa Mudigere, Jorge Nocedal, Mikhail Smelyanskiy, and Ping Tak Peter Tang. On large-batch training for deep learning: Generalization gap and sharp minima. In *International Conference on Learning Representations*, 2017.
- Guang-He Lee, Yang Yuan, Shiyu Chang, and Tommi Jaakkola. Tight certificates of adversarial robustness for randomly smoothed classifiers. *Advances in Neural Information Processing Systems*, 32, 2019.
- Chak Tou Leong, Yi Cheng, Kaishuai Xu, Jian Wang, Hanlin Wang, and Wenjie Li. No two devils alike: Unveiling distinct mechanisms of fine-tuning attacks. *arXiv preprint arXiv:2405.16229*, 2024.
- Hao Li, Zheng Xu, Gavin Taylor, Christoph Studer, and Tom Goldstein. Visualizing the loss landscape of neural nets. *Advances in Neural Information Processing Systems*, 31, 2018.
- Mingjie Li, Wai Man Si, Michael Backes, Yang Zhang, and Yisen Wang. Salora: Safety-alignment preserved low-rank adaptation. *arXiv preprint arXiv:2501.01765*, 2025.
- Aixin Liu, Bei Feng, Bing Xue, Bingxuan Wang, Bochao Wu, Chengda Lu, Chenggang Zhao, Chengqi Deng, Chenyu Zhang, Chong Ruan, et al. Deepseek-v3 technical report. *arXiv preprint arXiv:2412.19437*, 2024a.
- Chaoyue Liu, Libin Zhu, and Mikhail Belkin. Loss landscapes and optimization in over-parameterized non-linear systems and neural networks. *Applied and Computational Harmonic Analysis*, 59:85–116, 2022.
- Qin Liu, Chao Shang, Ling Liu, Nikolaos Pappas, Jie Ma, Neha Anna John, Srikanth Doss, Llu s Marquez, Miguel Ballesteros, and Yassine Benajiba. Unraveling and mitigating safety alignment degradation of vision-language models. *arXiv preprint arXiv:2410.09047*, 2024b.
- Ekdeep Singh Lubana, Eric J Bigelow, Robert P Dick, David Krueger, and Hidenori Tanaka. Mechanistic mode connectivity. In *International Conference on Machine Learning*, pp. 22965–23004, 2023.
- Kaifeng Lyu, Haoyu Zhao, Xinran Gu, Dingli Yu, Anirudh Goyal, and Sanjeev Arora. Keeping llms aligned after fine-tuning: The crucial role of prompt templates. *arXiv preprint arXiv:2402.18540*, 2024.
- Aleksander Madry, Aleksandar Makelov, Ludwig Schmidt, Dimitris Tsipras, and Adrian Vladu. Towards deep learning models resistant to adversarial attacks. In *International Conference on Learning Representations*, 2018.
- Mark Chen Mark Chen, Mark Chen. Evaluating large language models trained on code. 2021.
- Ninareh Mehrabi, Palash Goyal, Christophe Dupuy, Qian Hu, Shalini Ghosh, Richard Zemel, Kai-Wei Chang, Aram Galstyan, and Rahul Gupta. Flirt: Feedback loop in-context red teaming. In *EMNLP*, 2023.
- Xin Men, Mingyu Xu, Qingyu Zhang, Bingning Wang, Hongyu Lin, Yaojie Lu, Xianpei Han, and Weipeng Chen. Shortgpt: Layers in large language models are more redundant than you expect. *arXiv preprint arXiv:2403.03853*, 2024.

- Jishnu Mukhoti, Yarin Gal, Philip HS Torr, and Puneet K Dokania. Fine-tuning can cripple your foundation model; preserving features may be the solution. *arXiv preprint arXiv:2308.13320*, 2023.
- Behnam Neyshabur, Ryota Tomioka, and Nathan Srebro. Norm-based capacity control in neural networks. In *Conference on Learning Theory*, pp. 1376–1401, 2015.
- OpenAI. Gpt-4 technical report. *arXiv*, 2023.
- Long Ouyang, Jeffrey Wu, Xu Jiang, Diogo Almeida, Carroll Wainwright, Pamela Mishkin, Chong Zhang, Sandhini Agarwal, Katarina Slama, Alex Ray, et al. Training language models to follow instructions with human feedback. *Advances in neural information processing systems*, 35:27730–27744, 2022.
- Sheng Y Peng, Pin-Yu Chen, Matthew Hull, and Duen H Chau. Navigating the safety landscape: Measuring risks in finetuning large language models. *Advances in Neural Information Processing Systems*, 37:95692–95715, 2024.
- Ethan Perez, Saffron Huang, Francis Song, Trevor Cai, Roman Ring, John Aslanides, Amelia Glaese, Nat McAleese, and Geoffrey Irving. Red teaming language models with language models. In *EMNLP*, 2022.
- Xiangyu Qi, Yi Zeng, Tinghao Xie, Pin-Yu Chen, Ruoxi Jia, Prateek Mittal, and Peter Henderson. Fine-tuning aligned language models compromises safety, even when users do not intend to! In *The Twelfth International Conference on Learning Representations*, 2023.
- Xiangyu Qi, Ashwinee Panda, Kaifeng Lyu, Xiao Ma, Subhrajit Roy, Ahmad Beirami, Prateek Mittal, and Peter Henderson. Safety alignment should be made more than just a few tokens deep. In *The Thirteenth International Conference on Learning Representations*, 2024.
- Domenic Rosati, Jan Wehner, Kai Williams, Łukasz Bartoszcze, David Atanasov, Robie Gonzales, Subhabrata Majumdar, Carsten Maple, Hassan Sajjad, and Frank Rudzicz. Representation noising effectively prevents harmful fine-tuning on llms. *arXiv e-prints*, pp. arXiv–2405, 2024.
- Hadi Salman, Jerry Li, Ilya Razenshteyn, Pengchuan Zhang, Huan Zhang, Sebastien Bubeck, and Greg Yang. Provably robust deep learning via adversarially trained smoothed classifiers. *Advances in Neural Information Processing Systems*, 32, 2019.
- Rico Sennrich. Neural machine translation of rare words with subword units. *arXiv preprint arXiv:1508.07909*, 2015.
- Leslie N Smith and Nicholay Topin. Exploring loss function topology with cyclical learning rates. *arXiv preprint arXiv:1702.04283*, 2017.
- Jacob Mitchell Springer, Sachin Goyal, Kaiyue Wen, Tanishq Kumar, Xiang Yue, Sadhika Malladi, Graham Neubig, and Aditi Raghunathan. Overtrained language models are harder to fine-tune. *arXiv preprint arXiv:2503.19206*, 2025.
- Mingjie Sun, Zhuang Liu, Anna Bair, and J Zico Kolter. A simple and effective pruning approach for large language models. *arXiv preprint arXiv:2306.11695*, 2023.
- Martin J Wainwright. *High-dimensional statistics: A non-asymptotic viewpoint*, volume 48. Cambridge university press, 2019.
- Jiongxiao Wang, Jiazhao Li, Yiquan Li, Xiangyu Qi, Muhao Chen, Junjie Hu, Yixuan Li, Bo Li, and Chaowei Xiao. Mitigating fine-tuning jailbreak attack with backdoor enhanced alignment. *arXiv e-prints*, pp. arXiv–2402, 2024a.
- Zhichao Wang, Bin Bi, Shiva Kumar Pentylala, Kiran Ramnath, Sougata Chaudhuri, Shubham Mehrotra, Xiang-Bo Mao, Sitaram Asur, et al. A comprehensive survey of llm alignment techniques: Rlhf, rlaf, ppo, dpo and more. *arXiv preprint arXiv:2407.16216*, 2024b.
- Alexander Wei, Nika Haghtalab, and Jacob Steinhardt. Jailbroken: How does llm safety training fail? *Advances in Neural Information Processing Systems*, 36, 2023a.

- Zeming Wei, Yifei Wang, and Yisen Wang. Jailbreak and guard aligned language models with only few in-context demonstrations. *arXiv preprint arXiv:2310.06387*, 2023b.
- Chengcan Wu, Zhixin Zhang, Zeming Wei, Yihao Zhang, and Meng Sun. Mitigating fine-tuning risks in llms via safety-aware probing optimization. *arXiv preprint arXiv:2505.16737*, 2025.
- An Yang, Baosong Yang, Beichen Zhang, Binyuan Hui, Bo Zheng, Bowen Yu, Chengyuan Li, Dayiheng Liu, Fei Huang, Haoran Wei, et al. Qwen2.5 technical report. *arXiv preprint arXiv:2412.15115*, 2024.
- Xianjun Yang, Xiao Wang, Qi Zhang, Linda Petzold, William Yang Wang, Xun Zhao, and Dahua Lin. Shadow alignment: The ease of subverting safely-aligned language models. *arXiv preprint arXiv:2310.02949*, 2023.
- Yihao Zhang, Hangzhou He, Jingyu Zhu, Huanran Chen, Yifei Wang, and Zeming Wei. On the duality between sharpness-aware minimization and adversarial training. *arXiv preprint arXiv:2402.15152*, 2024a.
- Yihao Zhang, Zeming Wei, Jun Sun, and Meng Sun. Adversarial representation engineering: A general model editing framework for large language models. In *The Thirty-eighth Annual Conference on Neural Information Processing Systems*, 2024b.
- Lianmin Zheng, Wei-Lin Chiang, Ying Sheng, Siyuan Zhuang, Zhanghao Wu, Yonghao Zhuang, Zi Lin, Zhuohan Li, Dacheng Li, Eric Xing, et al. Judging llm-as-a-judge with mt-bench and chatbot arena. *Advances in Neural Information Processing Systems*, 36, 2024.
- Andy Zou, Zifan Wang, Nicholas Carlini, Milad Nasr, J Zico Kolter, and Matt Fredrikson. Universal and transferable adversarial attacks on aligned language models. *arXiv preprint arXiv:2307.15043*, 2023.

**Algorithm 1** Gaussian-augmented Optimizer for Basin Enlargement (GO optimizer)

---

**Require:** Model  $f_{\theta}$ , dataset  $\mathcal{D}$ , perturbation variance  $\sigma^2$ , base optimizer (e.g., SGD or Adam)

- 1: **for** each gradient step **do**
- 2:   Sample mini-batch  $\{\mathbf{x}_i\}_{i=1}^B \sim \mathcal{D}$  and  $\{\epsilon_i \sim \mathcal{N}(\mathbf{0}, \sigma^2 \mathbf{I})\}_{i=1}^B$ .
- 3:   Compute gradient on perturbed parameters  $\nabla_{\theta} L_{\text{train}} = -\sum_{i=1}^B \nabla_{\theta} \log p(\mathbf{x}_i | \theta + \epsilon_i)$
- 4:   Update parameters  $\theta \leftarrow \text{Optimizer}(\theta, \nabla_{\theta} L_{\text{train}})$
- 5: **end for**
- 6: **return**  $\theta$

---

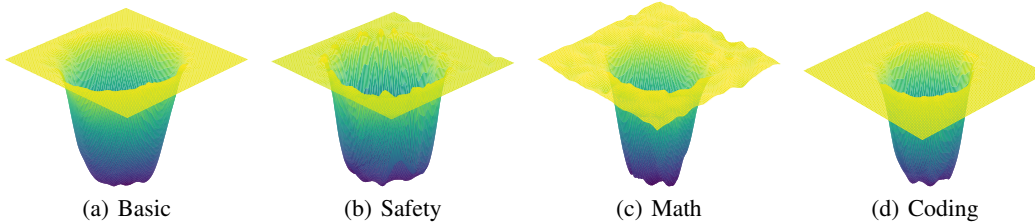


Figure 6: The 3D version of the most-case loss landscape, using Qwen2.5-7B model.

## A NOTATIONS

$d$	Number of parameters in a language model.
$\mathcal{D}$	Dataset for a benchmark.
$J_{\mathcal{D}}$	Benchmark that maps from $\mathbb{R}^d$ to $\mathbb{R}$ .
$\alpha$	Perturbation scale.
$\Phi$	CDF of the standard Gaussian distribution.
$\Phi^{-1}$	Inverse CDF of the standard Gaussian distribution.
$\theta$	Model’s parameters.
$\theta_0$	Model’s parameters before SFT.
$\theta_{sft}$	Model’s parameters after SFT.
$\sigma$	Basin size.
$e_i$	One-hot vector for token $i$ .
$\mathbf{W}$	The embedding matrix
$p_{\text{lower}}, p_{\text{upper}}$	Confidence interval obtained by Clopper Pearson Bound.

## B RELATED WORK

This work is greatly inspired by Peng et al. (2024), which argues that the safety loss landscape resembles a basin, within which the model is safe and outside of which it is not. Our study extends Peng et al. (2024) by investigating the loss landscape across additional capabilities and providing a deeper analysis of the relationship between loss landscapes and catastrophic forgetting during fine-tuning.

Concurrent work (Springer et al., 2025) suggests that over-pre-trained large language models are harder to fine-tune because they lack robustness to parameter perturbations using Gaussian noise. Our work complements this study by explaining how robustness to Gaussian parameter perturbations provides a lower bound on performance degradation during fine-tuning.

$\alpha (\times 10^{-3})$	0	0.5	1	1.5	2	2.5	3	3.5	4	4.5	5	5.5	6	6.5	7
Safety	1	1	1	0.98	0.98	0.98	0.98	0.98	0.98	0.98	0.96	0.78	0.06	0	0
Math	0.84	0.84	0.84	0.84	0.81	0.7	0.72	0.58	0.32	0.21	0.13	0.01	0	0	0
Basic	0.76	0.76	0.76	0.76	0.73	0.72	0.67	0.65	0.60	0.53	0.43	0.32	0.25	0.16	0
Coding	0.88	0.89	0.89	0.86	0.86	0.83	0.8	0.74	0.74	0.54	0.45	0.11	0	0	0

Table 1: The raw benchmark value  $J_{f, \mathcal{D}}(\theta + \alpha \delta)$  ( $\uparrow$ , the higher the better) of the most-case landscape using Qwen2.5-7B. Due to page limitations, we present only half of the data here. Thus, the basin size is twice as large as shown, accounting for (nearly) symmetric counterpart on the other side. As shown, the loss landscape literally forms basins, within these basins, the benchmark values remain literally unchanged.

## C WHY DO THE LOSS LANDSCAPES OF LLMs RESEMBLE BASINS?

This paper presents a seemingly different conclusion from Peng et al. (2024), where we argue that the loss landscape of large language models resembles a basin, whereas they suggest that LLM performance degrades gradually as the perturbation budget increases. The key reason is that Peng et al. (2024) uses benchmarks that evaluate models by log-likelihood, where the loss landscape is expected to be continuous and smooth (See Fig. 8(a)). In contrast, we use benchmarks that evaluate models based on their generation results.

This raises the question of why large language models perform nearly identically within a certain range of Gaussian perturbations to their parameters but rapidly lose all capabilities when perturbations exceed this range. This phenomenon aligns with recent findings that large language models can resist common noise perturbations (Men et al., 2024; Gromov et al., 2024; Sun et al., 2023), which show that removing certain modules in LLMs leaves their capabilities largely intact, but removing more causes a swift loss of conversational ability.

In this work, we do not have a definitive answer to this question. However, we hypothesize that this may stem from the over-parameterization property of LLMs. Mode connectivity is an important property of over-parameterized models, stating that the modes of an over-parameterized network are connected to one another (Garipov et al., 2018; Frankle et al., 2020; Lubana et al., 2023). For large language models, beyond permutation invariance in feed-forward networks (Ainsworth et al., 2022), there is also rotational invariance in key and query matrices. Consequently, these equivalent modes may be closer to each other, forming a subspace with dimensions nearly equivalent to the original space. We leave this exploration to future work.

## D MORE EXPERIMENTS

### D.1 MORE EXPERIMENTAL DETAILS

**Clarification on All Models Used in This Paper.** In this paper, we exclusively use the instructed or chat versions of models. We do not use any base models, as they are completely unable to engage in conversation and thus cannot be evaluated on any benchmark. Due to page limitations, we omit “instruct” or “chat” in the main text. For example, Qwen2.5-7B in the main text refers to Qwen2.5-7B-Instruct, not the pre-trained base model.

**Normalizing the Loss Landscape.** As described in Sec. 3.1, since benchmark values vary in scale and direction, we normalize each loss landscape to the interval  $[0, 1]$  and invert benchmarks where higher values indicate better performance, ensuring that lower values consistently represent better performance for unified visualization. This normalization involves three steps: first, subtracting the minimum value; then, dividing by the range to scale to  $[0, 1]$ ; and finally, inverting the value by computing one minus the normalized value.

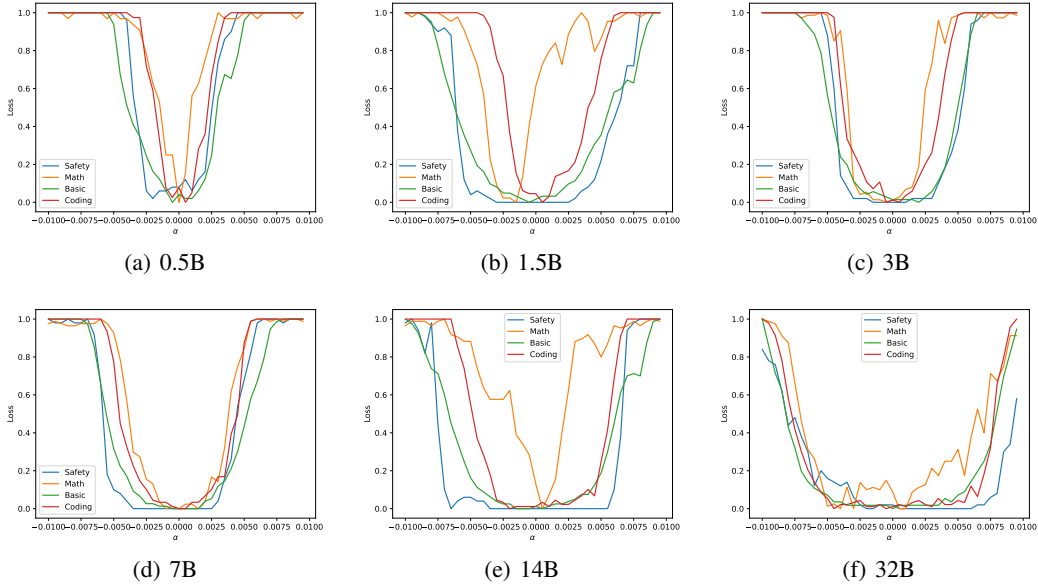


Figure 7: The most-case loss landscape of six Qwen2.5 models with different sizes. As shown, for the 0.5B model, the landscape resembles a small model and does not even resemble a basin. When the models become larger, the basins also become larger and clearer.

### D.2 RAW NUMERICAL VALUES OF BASINS

**Settings.** To better illustrate the basin phenomenon in the most-case loss landscape shown in Fig. 1, we provide the raw benchmark values for the Qwen2.5-7B model. Due to page limitations, we present data only for Qwen2.5-7B and include less than half of the perturbation range for  $\alpha$ , since the full dataset exhibiting near-symmetric behavior on the other side.

**Results.** As shown in Table 1, the most-case loss landscape of Qwen2.5-7B literally forms basins, where benchmark values remain completely unchanged within specific ranges of parameter perturbations. Specifically, for the Safety benchmark, the value remains constant at 1 for perturbations up to  $\alpha = 1 \times 10^{-3}$ , and for the Math and Basic benchmarks, the values are stable at 0.84 and 0.76, respectively, up to  $\alpha = 1.5 \times 10^{-3}$ . Similarly, the Coding benchmark shows near-constant values (0.88 to 0.89) up to  $\alpha = 1.5 \times 10^{-3}$ . This stability demonstrates that, within these basins, the model’s capabilities are entirely unaffected by random noise perturbations, aligning with our claim that the most-case landscape forms a robust basin structure, as visualized in Fig. 1.

### D.3 LOSS LANDSCAPES OF LARGE MODELS

We also visualize the loss landscapes of larger models, as shown in Fig. 7. We draw the following conclusions:

**Larger models tend to have larger basins.** As shown, for each capability, including basic, math, safety, and coding, the basin of Qwen2.5-0.5B is small, while that of Qwen2.5-7B is larger. Qwen2.5-32B has the largest basin, nearly twice the size of Qwen2.5-7B.

**Larger models have greater expressive power within their basins.** As analyzed in Sec. 4.3, the larger the model and its basin, the greater the expressive power within the basin. Since larger models have both more parameters and larger basin sizes (may due to their over-parameterized property), they exhibit significantly greater expressive power than smaller models.

**Larger models are more robust to fine-tuning and jailbreaking.** As analyzed in Sec. 4.1, the larger the basin size, the greater the robustness against fine-tuning and jailbreaking attacks. Therefore, we conclude that larger models are more robust to fine-tuning, less likely to compromise capabilities,

**Algorithm 2** Normalization of Benchmark Values ( $\mathcal{T}$ )

---

**Require:** Benchmark values  $\{J_{f,\mathcal{D}}(\boldsymbol{\theta} + \alpha\boldsymbol{\delta})\}_{\alpha \in A}$

- 1: Compute minimum value:  $\text{min\_val} \leftarrow \min_{\alpha} J_{f,\mathcal{D}}(\boldsymbol{\theta} + \alpha\boldsymbol{\delta})$
- 2: Compute maximum value:  $\text{max\_val} \leftarrow \max_{\alpha} J_{f,\mathcal{D}}(\boldsymbol{\theta} + \alpha\boldsymbol{\delta})$
- 3: Compute range:  $\text{range\_val} \leftarrow \text{max\_val} - \text{min\_val}$
- 4: Initialize normalized values:  $\text{normalized} \leftarrow []$
- 5: **for** each value  $\in \{J_{f,\mathcal{D}}(\boldsymbol{\theta} + \alpha\boldsymbol{\delta})\}_{\alpha \in A}$  **do**
- 6:   Scale to  $[0, 1]$ :  $\text{scaled} \leftarrow (\text{value} - \text{min\_val})/\text{range\_val}$
- 7:   Invert value:  $\text{inverted} \leftarrow 1 - \text{scaled}$
- 8:   Append to output:  $\text{normalized} \leftarrow \text{normalized} + [\text{inverted}]$
- 9: **end for**
- 10: **return** normalized

---

and more resistant to jailbreaking attacks. This may be one of the benefits of scaling up the model size.

## D.4 HYPOTHESIS TESTING WITH CLOPPER-PEARSON BOUND

**Soft Definition of Basins.** To verify the soft definition of basins (Definition 4.1), we aim to confirm whether  $J_{f,\mathcal{D}}(\boldsymbol{\theta}) - \mathbb{E}_{\epsilon \sim \mathcal{N}(\mathbf{0}, \sigma^2 \mathbf{I})}[J_{f,\mathcal{D}}(\boldsymbol{\theta} + \epsilon)] \leq \epsilon$ . We achieve this using the Clopper-Pearson bound by computing a confidence interval  $[p_{\text{lower}}, p_{\text{upper}}]$  for  $\mathbb{E}_{\epsilon \sim \mathcal{N}(\mathbf{0}, \sigma^2 \mathbf{I})}[J_{f,\mathcal{D}}(\boldsymbol{\theta} + \epsilon)]$  with a specified type-I error  $\gamma$ . Specifically, the Clopper-Pearson bound ensures that  $\mathbb{E}_{\epsilon \sim \mathcal{N}(\mathbf{0}, \sigma^2 \mathbf{I})}[J_{f,\mathcal{D}}(\boldsymbol{\theta} + \epsilon)] \in [p_{\text{lower}}, p_{\text{upper}}]$  with probability at least  $1 - \gamma$ . If  $J_{f,\mathcal{D}}(\boldsymbol{\theta}) - p_{\text{lower}} \leq \epsilon$ , we can assert, with type-I error  $\gamma$ , that the soft basin condition holds.

**Strict Definition of Basins.** For the strict definition of basins (Sec. 3.2), our goal is to estimate the proportion of directions where the normalized benchmark value is exactly 0, i.e., to compute a lower bound for  $\mathbb{E}_{\delta \sim \mathcal{N}(\mathbf{0}, \mathbf{I})}[\mathbb{I}\{\mathcal{T} \circ J_{f,\mathcal{D}}(\boldsymbol{\theta} + \alpha\boldsymbol{\delta}) = 0\}]$ . The Clopper-Pearson bound provides a confidence interval  $[p_{\text{lower}}, p_{\text{upper}}]$  with type-I error  $\gamma$ , allowing us to assert that at least  $p_{\text{lower}} \times 100\%$  of directions form a strict basin with probability  $1 - \gamma$ .

**Introduction to the Clopper-Pearson Bound.** The Clopper-Pearson bound constructs exact confidence intervals for the success probability  $p$  of a binomial distribution, ensuring strict control over the type-I error rate  $\gamma$ , i.e., the probability of rejecting a true null hypothesis. Unlike approximate methods (e.g., normal approximation), it leverages the binomial likelihood and the Beta distribution to compute precise bounds, making it ideal for estimating basin sizes in large language models where accurate error control is critical.

**Formulation and Application.** Let  $X$  denote a binomial random variable representing the number of successes in  $n$  independent Bernoulli trials, where a success indicates that the perturbed model  $f_{\boldsymbol{\theta} + \epsilon}$  retains performance comparable to the original model  $f_{\boldsymbol{\theta}}$ . For the strict basin (Sec. 3.2), a success occurs when  $\mathcal{T} \circ J_{f,\mathcal{D}}(\boldsymbol{\theta} + \alpha\boldsymbol{\delta}) = 0$ . For the soft basin (Theorem 4.1), since  $J_{f,\mathcal{D}}(\boldsymbol{\theta} + \epsilon)$  is also an expectation of the Bernoulli variable (i.e., 0-1 loss on each instance) over  $\mathcal{D}$ , a success occurs when the answer of a sampled instance is judged as "correct" or "safe". Given a confidence level  $1 - \gamma$  (we use  $\gamma = 0.01$ ), the Clopper-Pearson confidence interval  $[p_{\text{lower}}, p_{\text{upper}}]$  for  $p$  is defined by:

$$P(X \geq x \mid p = p_{\text{lower}}) = \frac{\gamma}{2}, \quad (9)$$

$$P(X \leq x \mid p = p_{\text{upper}}) = \frac{\gamma}{2}, \quad (10)$$

where  $x$  is the observed number of successes in  $n$  trials. These bounds are computed using the inverse of the regularized incomplete Beta function:

$$p_{\text{lower}} = I_{x, n-x+1}^{-1}\left(\frac{\gamma}{2}\right), \quad (11)$$

$$p_{\text{upper}} = I_{x+1, n-x}^{-1}\left(1 - \frac{\gamma}{2}\right), \quad (12)$$

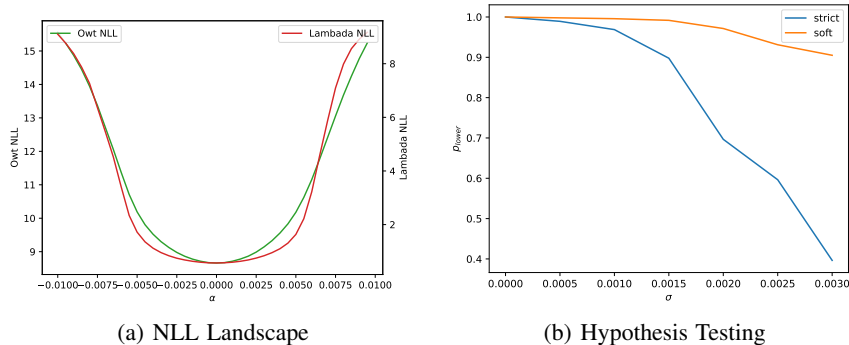


Figure 8: Loss landscape and hypothesis testing results using a likelihood-based benchmark. (a) The loss landscape of Qwen2.5-7B for a likelihood-based benchmark is smooth and continuous. (b) The lower bound  $p_{\text{lower}}$  from the Clopper-Pearson bound for the soft basin definition (i.e., the lower bound for  $\mathbb{E}_{\epsilon \sim \mathcal{N}(\mathbf{0}, \sigma^2 \mathbf{I})} [J_{f, \mathcal{D}}(\boldsymbol{\theta} + \epsilon)]$ ) and the strict basin definition (i.e., the lower bound for proportion of directions achieving the exact zero loss).

where  $I_{a,b}(z)$  is the cumulative distribution function of the Beta distribution  $\text{Beta}(a, b)$ . This ensures that our estimation of basin size maintains a type-I error rate below 0.01, providing a robust foundation for theoretical and experimental analyses.

**Experimental Settings.** Following Cohen et al. (2019); Salman et al. (2019); Chen et al. (2025a), we use Monte Carlo sampling with the Clopper-Pearson bound to estimate basin sizes. We set a type-I error of  $\gamma = 0.01$  and a sample size of  $n = 100,000$  to ensure precise confidence intervals. For the soft basin, we evaluate  $J_{f, \mathcal{D}}(\boldsymbol{\theta} + \epsilon)$  with  $\epsilon \sim \mathcal{N}(\mathbf{0}, \sigma^2 \mathbf{I})$  and  $\sigma = 0.01$ , and obtain the statistical lower bound for  $\mathbb{E}_{\epsilon \sim \mathcal{N}(\mathbf{0}, \sigma^2 \mathbf{I})} [J_{f, \mathcal{D}}(\boldsymbol{\theta} + \epsilon)]$ . For the strict basin, we sample directions  $\boldsymbol{\delta} \sim \mathcal{N}(\mathbf{0}, \mathbf{I})$  and compute  $\mathcal{T} \circ J_{f, \mathcal{D}}(\boldsymbol{\theta} + \alpha \boldsymbol{\delta})$  with  $\alpha \in [0, 3 \times 10^{-3}]$ , as in Table 1. These settings enable reliable validation of the most-case basin properties, as visualized in Fig. 1.

**Experimental Results.** The statistical lower bounds obtained for both the strict and soft definitions of basins are shown in Fig. 8(b). As demonstrated, the lower bound for the soft basin definition significantly exceeds that of the strict basin definition, aligning with our observation that when  $\epsilon \rightarrow 0$  in Definition 4.1, the soft definition becomes the strict definition of basins, assuming the expected loss does not decrease after adding noise. We present the respective conclusions for the two definitions as follows:

**Results for Strict Definition of Basins.** In the strict definition of basins, the lower bound  $p_{\text{lower}}$  represents the proportion of directions forming strict basins. As shown in Fig. 8(b), for  $\sigma = 0.01$ , we can assert that more than 90% of directions form strict basins, whereas for  $\sigma = 0.02$ , we can assert that more than 65% of directions form strict basins. As  $\sigma$  increases, the proportion of directions that form strict basins decreases.

**Results for Soft Definition of Basins.** In the soft definition of basins, the lower bound  $p_{\text{lower}}$  provides a statistical guarantee for  $\mathbb{E}_{\epsilon \sim \mathcal{N}(\mathbf{0}, \sigma^2 \mathbf{I})} [J_{f, \mathcal{D}}(\boldsymbol{\theta} + \epsilon)]$ . As demonstrated, larger  $\sigma$  values lead to worse model performance under noise perturbations but reduce the Lipschitz constant of the smoothed model. This reflects a classical robustness-accuracy tradeoff in randomized smoothing (Cohen et al., 2019; Salman et al., 2019; Chen et al., 2024). Choosing a larger  $\sigma$  enhances model robustness but may compromise accuracy, potentially resulting in either improved or degraded performance. In Sec. 4, we select  $\sigma = 0.03$ , for which  $p_{\text{lower}}$  remains above 0.9.

## D.5 PRETRAINING USING GO OPTIMIZER

To evaluate the effectiveness of the GO optimizer, we conducted pre-training and fine-tuning experiments on a GPT2-127M model, as detailed in Table 2. The key findings are summarized below.

**Low Computational Overhead of GO Optimizer in Pre-training.** During pre-training on OpenWebText for 300,000 steps, the GO optimizer introduces minimal computational overhead compared

Table 2: Evaluation of models pretrained by 300k steps with AdamW and GO optimizers, then fine-tuned with AdamW optimizer. The GO optimizer effectively prevents forgetting during supervised fine-tuning while maintaining comparable performance during pretraining.

Model	OWT NLL ( $\downarrow$ )	Lambada PPL ( $\downarrow$ )	Lambada ACC	HellaSwag	SST2	WinoGrande	ARC-E	ARC-C
GPT-2-Official	3.11	38.6	30.6	38.9	56.7	51.3	43.1	17.2
AdamW-300k	<b>2.94</b>	<b>38.3</b>	32.4	<b>40.2</b>	51.4	50.9	<b>44.1</b>	18.2
GO-300k	2.97	40.8	<b>32.9</b>	38.0	<b>57.7</b>	<b>51.6</b>	41.2	<b>18.9</b>
AdamW-SFT	3.49	94.1	26.8	<b>39.8</b>	51.7	49.8	<b>44.0</b>	<b>23.6</b>
GO-SFT	<b>3.37</b>	<b>80.1</b>	<b>28.3</b>	37.8	<b>57.1</b>	<b>51.1</b>	42.8	21.8

to AdamW. As shown in Fig. 5(a), the GO optimizer is initially slower due to its optimization over the entire parameter neighborhood, resulting in a negative log-likelihood (NLL) of 2.97 compared to AdamW’s 2.94, a marginal gap of 0.03. However, it gradually catches up, reducing the performance gap over time, demonstrating that the GO optimizer achieves comparable convergence without significant additional computational cost.

**Implicit Biases Beyond Basin Enlargement.** The GO optimizer exhibits implicit biases that extend beyond enlarging the most-case basin, leading to superior performance on specific benchmarks. As shown in Table 2, the GO optimizer outperforms AdamW on LAMBADA accuracy (32.9 vs. 32.4), SST-2 (57.7 vs. 51.4), WinoGrande (51.6 vs. 50.9), and ARC-C (18.9 vs. 18.2) after 300,000 pre-training steps. These improvements suggest that the GO optimizer introduces beneficial inductive biases, enhancing model generalization on certain tasks.

**Effective Prevention of Forgetting During Fine-tuning.** In the fine-tuning phase on the Alpaca dataset using the AdamW optimizer, the GO-pre-trained model significantly mitigates forgetting of prior capabilities compared to the AdamW-pre-trained model. Although AdamW initially achieves better performance on some benchmarks during pre-training (e.g., OpenWebText NLL of 2.94 vs. 2.97), fine-tuning reveals substantial forgetting in the AdamW-pre-trained model, with OpenWebText NLL degrading to 3.49, compared to 3.37 for the GO-pre-trained model—a gap of 0.12. Similar trends are observed in LAMBADA perplexity (94.1 vs. 80.1) and accuracy (26.8 vs. 28.3), as shown in Table 2, confirming that the GO optimizer effectively preserves prior capabilities during supervised fine-tuning.

## D.6 ABOUT NORM CONSTRAINTS IN LANDSCAPE VISUALIZATION

One might argue that the norm constraint should be  $\|\delta\|_2 = \mathbb{E}[\|\mathcal{N}(\mathbf{0}, \mathbf{I})\|_2]$  instead of  $\|\delta\|_2^2 = \mathbb{E}[\|\mathcal{N}(\mathbf{0}, \mathbf{I})\|_2^2]$ . By Jensen’s inequality,  $\mathbb{E}[\|\mathcal{N}(\mathbf{0}, \mathbf{I})\|_2^2] \geq \mathbb{E}[\|\mathcal{N}(\mathbf{0}, \mathbf{I})\|_2]^2$ . However, these two constraints become equivalent as  $d \rightarrow \infty$ . For the high-dimensional spaces typical of large language models, these constraints are nearly identical.

This is because  $\mathbb{E}[\|\mathcal{N}(\mathbf{0}, \mathbf{I})\|_2^2] - \mathbb{E}[\|\mathcal{N}(\mathbf{0}, \mathbf{I})\|_2]^2 = \text{Var}(\|\mathcal{N}(\mathbf{0}, \mathbf{I})\|_2) = \frac{1}{2} + O\left(\frac{1}{d}\right)$ . Thus, the relative error  $\frac{\text{Var}(\|\mathcal{N}(\mathbf{0}, \mathbf{I})\|_2)}{\mathbb{E}[\|\mathcal{N}(\mathbf{0}, \mathbf{I})\|_2]^2}$  approaches zero at a rate of  $O(1/d)$ .

## D.7 NORM OF COMMON FINE-TUNING

We also test the  $\ell_2$  norm of common post-training techniques to determine whether they are located within basins or guaranteed regions. As shown in Table 3, we draw the following conclusions:

**Common fine-tuning configurations are all located within the original basin.** As shown, the  $\ell_2$  norm of the basin size is approximately 250.99. All common fine-tuning configurations are located within basins. For reference, the  $\ell_2$  norm between two distinct pre-trained models, Qwen2.5-Math-7B and Qwen2.5-7B, is much larger than this distance. This verifies our claim that benign fine-tuning within the basin does not compromise capabilities.

**Larger learning rates lead to greater fine-tuning distances and a higher likelihood of catastrophic forgetting.** As shown, the larger the learning rate, the more likely the optimizer is to favor

Table 3: The distance of different tuning configurations and whether they are located in basin and guaranteed regions. As shown, fine-tuning configurations are always within the basin but not the guaranteed region.

Model	Tuning Configs	Basin Size	Tuning Distance	Guaranteed Region
Qwen2.5-7B	Qwen2.5-7B-1M	$0.003 \cdot \sqrt{7B}$	152.06	0.1
Qwen2.5-7B	Qwen2.5-7B-Base	$0.003 \cdot \sqrt{7B}$	25.98	0.1
Qwen2.5-Math-7B	DeepSeek-Distill	$0.003 \cdot \sqrt{7B}$	358.99	0.1
Qwen2.5-7B	Qwen2.5-Math-7B	$0.003 \cdot \sqrt{7B}$	1820.83	0.1
Qwen2.5-7B	Alpaca lr=5e-5	$0.003 \cdot \sqrt{7B}$	100.87	0.1
Qwen2.5-7B	Alpaca lr=2e-5	$0.003 \cdot \sqrt{7B}$	37.87	0.1
Qwen2.5-7B	AdvBench lr=5e-5	$0.003 \cdot \sqrt{7B}$	26.91	0.1

solutions with greater distances. Consequently, such configurations are more likely to compromise capabilities.

**Common fine-tuning configurations are not located within the guaranteed region.** As shown, the theoretical guaranteed region is small enough to prevent capability compromise. This is because the theoretical guaranteed region serves only as a lower bound, i.e., only when fine-tuning along the worst-case direction does moving outside the guaranteed region compromise capabilities. Since normal fine-tuning does not align with worst-case directions, it typically has a much larger fine-tuning distance budget than these guaranteed lower bounds.

## E PROOF OF THEOREM 4.2 AND THEOREM 4.3

### E.1 PROOF OF THEOREM 4.3

In this section, we present a simplified proof of Theorem 4.3 by adapting Lemma 2 from Salman et al. (2019). We first restate this lemma:

**Lemma E.1** *For any function  $f : \mathbb{R}^d \rightarrow \mathbb{R}$ , the map  $\mathbf{x} \rightarrow \Phi^{-1}(\mathbb{E}_{\epsilon \sim \mathcal{N}(\mathbf{0}, \mathbf{I})}[f(\mathbf{x} + \epsilon)])$  is at most 1-Lipschitz.*

By setting  $J_{\mathcal{D}}$  as  $f$  and  $\boldsymbol{\theta}$  as  $\mathbf{x}$ , we establish that, for any benchmark function  $J_{\mathcal{D}} : \mathbb{R}^d \rightarrow \mathbb{R}$ , the map  $\boldsymbol{\theta} \rightarrow \Phi^{-1}(\mathbb{E}_{\epsilon \sim \mathcal{N}(\mathbf{0}, \mathbf{I})}[J_{\mathcal{D}}(\boldsymbol{\theta} + \epsilon)])$  is 1-Lipschitz. Consequently, we consider the function:

$$\begin{aligned} \Phi^{-1}(\mathbb{E}_{\epsilon \sim \mathcal{N}(\mathbf{0}, \sigma^2 \mathbf{I})}[J_{\mathcal{D}}(\boldsymbol{\theta} + \epsilon)]) &= \Phi^{-1}(\mathbb{E}_{\epsilon \sim \mathcal{N}(\mathbf{0}, \mathbf{I})}[J_{\mathcal{D}}(\boldsymbol{\theta} + \sigma \cdot \epsilon)]) \\ &= \Phi^{-1}\left(\mathbb{E}_{\epsilon \sim \mathcal{N}(\mathbf{0}, \mathbf{I})}\left[J_{\mathcal{D}}\left(\sigma \cdot \left(\frac{\boldsymbol{\theta}}{\sigma} + \epsilon\right)\right)\right]\right), \end{aligned}$$

which is at most 1-Lipschitz with respect to  $\frac{\boldsymbol{\theta}}{\sigma}$ , implying that it is at most  $\frac{1}{\sigma}$ -Lipschitz with respect to  $\boldsymbol{\theta}$ . Thus, we obtain:

$$\Phi^{-1}(\mathbb{E}_{\epsilon \sim \mathcal{N}(\mathbf{0}, \sigma^2 \mathbf{I})}[J_{\mathcal{D}}(\boldsymbol{\theta}_{sft} + \epsilon)]) \geq \Phi^{-1}(\mathbb{E}_{\epsilon \sim \mathcal{N}(\mathbf{0}, \sigma^2 \mathbf{I})}[J_{\mathcal{D}}(\boldsymbol{\theta}_0 + \epsilon)]) - \frac{\|\boldsymbol{\theta}_{sft} - \boldsymbol{\theta}_0\|_2}{\sigma}.$$

By applying  $\Phi$  to both sides, we derive:

$$\mathbb{E}_{\epsilon \sim \mathcal{N}(\mathbf{0}, \sigma^2 \mathbf{I})}[J_{\mathcal{D}}(\boldsymbol{\theta}_{sft} + \epsilon)] \geq \Phi\left(\Phi^{-1}(\mathbb{E}_{\epsilon \sim \mathcal{N}(\mathbf{0}, \sigma^2 \mathbf{I})}[J_{\mathcal{D}}(\boldsymbol{\theta}_0 + \epsilon)]) - \frac{\|\boldsymbol{\theta}_{sft} - \boldsymbol{\theta}_0\|_2}{\sigma}\right),$$

which matches the result of Theorem 4.3.

### E.2 PROOF OF THEOREM 4.2

Researchers have provided various methods to prove Theorem 4.2, e.g., through the Neyman-Pearson Lemma (Cohen et al., 2019), knapsack algorithm (Chen et al., 2025a), and Lipschitz prop-

erties (Salman et al., 2019; Chen et al., 2024). In this section, we deduce Theorem 4.2 from Theorem 4.3, avoiding repetition of previous proofs and providing a more direct connection between these theorems.

$$\begin{aligned}
& \boldsymbol{\theta} \rightarrow \Phi^{-1} \left( \mathbb{E}_{\epsilon \sim \mathcal{N}(\mathbf{0}, \sigma^2 \mathbf{I})} [J_{\mathcal{D}}(\boldsymbol{\theta} + \epsilon)] \right) \text{ is } \frac{1}{\sigma}\text{-Lipschitz} \\
& \iff \left\| \nabla_{\boldsymbol{\theta}} \Phi^{-1} \left( \mathbb{E}_{\epsilon \sim \mathcal{N}(\mathbf{0}, \sigma^2 \mathbf{I})} [J_{\mathcal{D}}(\boldsymbol{\theta} + \epsilon)] \right) \right\| \leq \frac{1}{\sigma} \\
& \iff \frac{\left\| \nabla_{\boldsymbol{\theta}} \mathbb{E}_{\epsilon \sim \mathcal{N}(\mathbf{0}, \sigma^2 \mathbf{I})} [J_{\mathcal{D}}(\boldsymbol{\theta} + \epsilon)] \right\|}{\Phi' \left( \mathbb{E}_{\epsilon \sim \mathcal{N}(\mathbf{0}, \sigma^2 \mathbf{I})} [J_{\mathcal{D}}(\boldsymbol{\theta} + \epsilon)] \right)} \leq \frac{1}{\sigma} \\
& \implies \frac{\left\| \nabla_{\boldsymbol{\theta}} \mathbb{E}_{\epsilon \sim \mathcal{N}(\mathbf{0}, \sigma^2 \mathbf{I})} [J_{\mathcal{D}}(\boldsymbol{\theta} + \epsilon)] \right\|}{\frac{1}{\sqrt{2\pi}}} \leq \frac{1}{\sigma} \\
& \implies \left\| \nabla_{\boldsymbol{\theta}} \mathbb{E}_{\epsilon \sim \mathcal{N}(\mathbf{0}, \mathbf{I})} [J_{\mathcal{D}}(\boldsymbol{\theta} + \epsilon)] \right\| \leq \frac{1}{\sqrt{2\pi}\sigma} \\
& \implies \mathbb{E}_{\epsilon \sim \mathcal{N}(\mathbf{0}, \mathbf{I})} [J_{\mathcal{D}}(\boldsymbol{\theta} + \epsilon)] \text{ is at most } \frac{1}{\sqrt{2\pi}\sigma}\text{-Lipschitz}
\end{aligned}$$

### E.3 COMPARISON OF THEOREM 4.2 AND THEOREM 4.3

Beyond the fact that Theorem 4.3 is strictly stronger than Theorem 4.2 (i.e., the Lipschitz constant of Theorem 4.3 at each point is strictly less than  $\frac{1}{\sqrt{2\pi}\sigma}$ ), there is also a significant difference. Theorem 4.3 indicates that the higher the clean accuracy  $p_A$ , the smaller the Lipschitz constant, and thus the greater the robustness; when  $p_A = 1$ , the Lipschitz constant becomes zero, making forgetting extremely unlikely. Conversely, the lower the clean accuracy  $p_A$ , the larger the Lipschitz constant, and the more likely performance degradation occurs. This eliminates the forgetting-learning tradeoff even along the worst-case direction, i.e., as long as the performance on old tasks exceeds that on new tasks, the smoothness constraints make it more likely to learn new tasks than to forget old tasks, and the performance degradation on old tasks is always less than the maximum performance gain on new tasks.

## F LIMITATIONS AND FUTURE WORK

In this work, we discovered the emergence of basins: as models grow larger, they exhibit absolute robustness to Gaussian noise within a certain range, resulting in the formation of basins (Sec. 3.2). Based on this, we conjecture that *as long as benign fine-tuning occurs within the basin, the model will not forget existing capabilities*. The reasoning for this conjecture is: *If random directions are minimally harmful within a certain range, forming a basin of stability, benign fine-tuning directions should be no more harmful than random perturbations*. We experimentally validated that benign fine-tuning behaves this way (Sec. 3.4). More rigorously, we used randomized smoothing techniques to prove that, if the model has a  $\sigma$ -basin, performance degradation during benign fine-tuning can be bounded, providing a rigorous theoretical explanation for the conjecture (Sec. 4.1). Additional contributions include: analyzing how parameter space robustness provides loose guarantees against jailbreaking attacks (Sec. 4.2), exploring whether a regularization term could constrain supervised fine-tuning (SFT) within the basin in the future (Sec. 4.3), and conducting a preliminary investigation into simple methods to enlarge the basin (Sec. 5).

### F.1 RANDOMIZED SMOOTHING REGIME

As models grow larger, we draw the following conclusions:

- As models grow larger, their basins naturally expand, increasing the theoretically guaranteed radius (which is  $O(\sigma)$ ) for subsequent fine-tuning, making it harder to compromise prior capabilities.
- As models and their basins grow larger, the regions within the basin exhibit greater expressive power, facilitating the acquisition of new capabilities.

We define the region where the model is guaranteed to preserve prior capabilities while learning new capabilities as the Randomized Smoothing Regime (RS Regime). The region where the model is guaranteed to preserve prior capabilities has a size of  $O(\sigma)$  (see Sec. 4.1). Taking Rademacher complexity as a metric for expressive power, for the expressive power to exceed  $k$ , we require  $O(d\sigma^2) \geq k \iff \sigma \geq O\left(\sqrt{\frac{k}{d}}\right)$ . Thus, the RS Regime is  $[0, O(\sigma)] \cap \left[O\left(\sqrt{\frac{k}{d}}\right), +\infty\right)$ . As models grow larger,  $O(\sigma)$  continues to grow, while  $O\left(\sqrt{\frac{k}{d}}\right)$  continues to decrease. Consequently, the RS Regime, representing the theoretically guaranteed region for preserving prior capabilities and acquiring new capabilities, continuously expands. When models have infinitely many parameters, all fine-tuning may lie within the RS Regime, analogous to the Neural Tangent Kernel (NTK) regime (Jacot et al., 2018), where infinitely wide models behave like kernel methods. Future work could explore how quickly models enter the RS Regime as their size increases and identify when this transition occurs.

## F.2 LARGER SCALE PRE-TRAINING STUDIES

Although we conducted pre-training studies using the GO optimizer, the scale is limited to the NanoGPT level, and several questions remain unanswered:

- As the model size increases, does it become easier or harder to expand the basin? Will the maximum basin size increase or decrease? Will the optimization speed increase or decrease? Addressing these questions may require a scaling law for basin size with respect to the number of training data and parameters.
- As the data composition becomes more complex and the number of parameters increases, does the GO optimizer still introduce implicit biases beyond enlarging basins, as observed in Sec. D.5? Will these biases remain benign or become harmful?

In the future, we plan to conduct pre-training studies on the GO optimizer at a much larger scale, e.g., on 7B models and 10T training data.